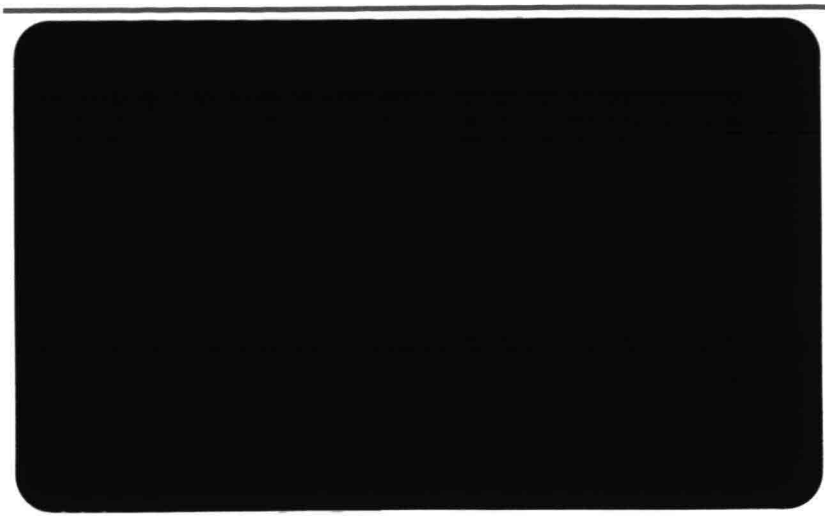

TU Delft

Delft University of Technology

Faculty of Civil Engineering
Hydraulic Engineering

Local Scour

Flow simulation by the

2-D turbulent model

ODYSSEE

report nr. 2-88

Faculty of Civil Engineering
Hydraulic Engineering
Delft University of Technology
1988

Contents

Figures

Notation

C	Chezy coefficient	$[L^{1/2}T^{-1}]$
c_d	empirical constant	[-]
c_f	friction coefficient	[-]
c_k	constant in k-model	[-]
$c_{1\epsilon}$	constant in turbulence model (k-ϵ)	[-]
$c_{2\epsilon}$	constant in turbulence model (k-ϵ)	[-]
c_μ	constant in turbulence model (k-ϵ)	[-]
f	roughness parameter or function	[-]
Fr	Froude number	[-]
g	acceleration of gravity	$[LT^{-2}]$
h	flow depth	[L]
H	step height	[L]
k	turbulent kinetic energy per unit mass	$[L^2T^{-2}]$
k_s	equivalent roughness of Nikuradse	[L]
l_m	mixing length (Prandtl)	[L]
M	mass flow rate per unit width	$[MT^{-1}]$
P	stress production of k	$[L^2T^{-3}]$
$\bar{p}$	time-averaged static fluid pressure	$[ML^{-1}T^{-2}]$
p^1	fluid pressure fluctuation	$[ML^{-1}T^{-2}]$
Q	discharge	$[L^3T^{-1}]$
q	discharge per unit width	$[L^2T^{-1}]$
Re	Reynolds number	[-]
r_t	depth averaged turbulence	[-]
$\bar{u}$	longitudinal mean flow (local) or depth-averaged velocity	$[LT^{-1}]$
u^1	longitudinal flow velocity fluctuation	$[LT^{-1}]$
u_*	friction velocity	$[LT^{-1}]$
v^1	lateral flow velocity fluctuation	$[LT^{-1}]$
$\bar{w}$	vertical mean flow velocity	$[LT^{-1}]$
w^1	vertical flow velocity fluctuation	$[LT^{-1}]$
x	longitudinal coordinate	[L]
x_R	reattachment length	[L]
y	lateral coordinate	[L]
z	vertical coordinate	[L]
z_o	zero-velocity level	[L]

Notation (continued)

δ	displacement thickness or shear-layer distance	[L]
θ	momentum thickness of a boundary layer	[L]
ϵ	rate of energy dissipation per unit mass by turbulence	$[L^2 T^{-3}]$
κ	constant of Von Karman	[-]
ν	kinematic molecular coefficient	$[L^2 T^{-1}]$
ν_t	eddy viscosity coefficient	$[L^2 T^{-1}]$
ρ	fluid density	$[ML^{-3}]$
σ_k	constant in turbulence model (k-ϵ)	[-]
σ_ϵ	constant in turbulence model (k-ϵ)	[-]
τ_t	turbulent shear stress	$[ML^{-1} T^{-2}]$
τ_o	bottom shear stress	$[ML^{-1} T^{-2}]$

Subscripts

s	at surface
max	maximum
n	normal
o	at initial section (x = 0)
t	turbulent
τ	longitudinal (tangential)

1.0 Introduction

The general purpose of this research project is to model mathematically the local scour downstream of a structure (2-D). The model has to simulate the development of the scour as a function of the time.

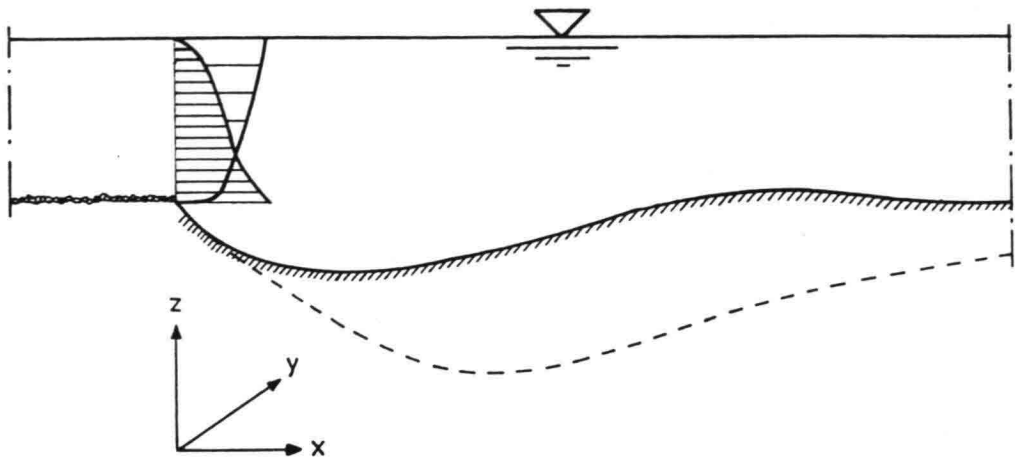

Figure A Lay-out of a local scour

Basically two models are necessary namely a flow model and a morphological model. The latter model has to describe the bed and suspended load and the erosion of the bottom. The choice which model has to be used, depends on the required accuracy and the computer costs.

In the present study a mathematical model is described which is based on the two-dimensional unsteady Reynolds equations for the mean flow. The turbulence closure is obtained by use of a two-dimensional model for the transport of the turbulence energy (k) and its dissipation (ϵ). Experimental data concerning the flow in a number of local scours (Breusers) and in a backward-facing step (Nezu) have been used to verify the model using a standard set of constants.
Also a description of the k-model (Jorissen) is given, which is a simplification of the k-ϵ-model. The results of this model are compared with k-ϵ calculations.

The mathematical and numerical modelling of the k-ϵ-model has been done by the 'Laboratoire National d'Hydraulique', a department of the 'Electricite de France', Chatou in France and Delft Hydraulics.

The modelling of the k-model has been done by the Delft University of Technology, Department of Civil Engineering.
The project is sponsored by the Dutch Department of Public Works Rijkswaterstaat, Bouwspeurwerk.
The present report has been composed by G.J.C.M. Hoffmans.

2.0 k-ϵpsilon-model

2.1 Assumptions and equations

The k-ϵ-model (two-dimensional vertical) is a model which is based on six mathematical equations with six unknown variables and a standard set of five basic constants. In addition to the equation of continuity and the two equations of motion in the longitudinal and verical direction respectively the set equations also contains the kinetic energy (k) and the dissipation (ϵ) transport equations and the relation between the eddy viscosity and the parameters mentioned above.
The exact equations for the transport of k and ϵ are derived from the Navier-Stokes equations. Because of the fairly drastic model assumptions these equations are not of too much relevance for this review and will not be given here.
The flow will be considered incrompressible and steady. Then the following equations apply.

continuity

$$\frac{\partial \bar{u}}{\partial x} + \frac{\partial \bar{w}}{\partial z} = 0 \qquad (1)$$

motion

$$\frac{\partial \bar{u}^2}{\partial x} + \frac{\partial \overline{uw}}{\partial z} = -\frac{\partial}{\rho \partial x}(\bar{p} - \tau_{xx}) + \frac{\partial}{\rho \partial z}(\tau_{zx}) \qquad (2)$$

$$\frac{\partial \overline{uw}}{\partial x} + \frac{\partial \bar{w}^2}{\partial z} = -\frac{\partial}{\rho \partial z}(\bar{p} - \tau_{zz}) + \frac{\partial}{\rho \partial x}(\tau_{xz}) + g \qquad (3)$$

in which:

$\bar{u}$ = time-averaged fluid velocity in x direction
$\bar{w}$ = time-averaged fluid velocity in z direction
$\bar{p}$ = time-averaged static fluid pressure
τ_n = normal stress component (τ_{xx},τ_{zz})
τ_τ = (tangential) shear stress component (τ_{zx},τ_{xz})
x = longitudinal coordinate
z = vertical coordinate
ρ = fluid density
g = acceleration of gravity

The normal and shear stresses represent a viscous and a fluctuating (turbulence) part. These stresses are defined as:

$$\tau_{xx} = 2\rho\nu\frac{\partial\bar{u}}{\partial x} - \rho\overline{u^1u^1} \tag{4}$$

$$\tau_{zz} = 2\rho\nu\frac{\partial\bar{w}}{\partial z} - \rho\overline{w^1w^1} \tag{5}$$

$$\tau_{zx} = \tau_{xz} = \rho\nu(\frac{\partial\bar{u}}{\partial z} + \frac{\partial\bar{w}}{\partial x}) - \rho\overline{u^1w^1} \tag{6}$$

in which:
ν = kinematic viscosity
u^1 = turbulent velocity in x-direction
w^1 = turbulent velocity in z-direction

The turbulent or Reynolds stresses are modelled in a way analogous to the viscous stresses according to the hypothesis of Boussinesq, see Rodi (1980).

$$\tau_{t,xx} = -\rho\overline{u^1u^1} = 2\rho\nu_t\frac{\partial\bar{u}}{\partial x} - \frac{2}{3}\rho k \tag{7}$$

$$\tau_{t,zz} = -\rho\overline{w^1w^1} = 2\rho\nu_t\frac{\partial\bar{w}}{\partial z} - \frac{2}{3}\rho k \tag{8}$$

$$\tau_{t,zx} = \tau_{t,xz} = -\rho\overline{u^1w^1} = \rho\nu_t\{\frac{\partial\bar{u}}{\partial z} + \frac{\partial\bar{w}}{\partial x}\} \tag{9}$$

in which:
$\tau_{t,n}$ = turbulent normal stress ($\tau_{t,xx}$,$\tau_{t,zz}$)
$\tau_{t,\tau}$ = turbulent (tangential) shear stress ($\tau_{t,zx}$,$\tau_{t,xz}$)
ν_t = eddy viscosity
k = turbulent kinetic energy per unit mass

Neglecting the viscous stresses, the equations of continuity and motion can be solved numerically provided the eddy viscosity is specified. The viscous effects are only important in the case of a viscous sub-layer. Then empirical laws of sufficient generality are available (logarithmic velocity) that relate the wall conditions to the conditions just outside the viscous sub-layer.
The two-equation (turbulence) closure is based on the transport equations for the turbulent kinetic energy (k) and its dissipation (ϵ). The exact k and ϵ are defined as:

$$k = \{\overline{(u^1)^2} + \overline{(v^1)^2} + \overline{(w^1)^2}\}/2 \tag{10}$$

$$\epsilon = \nu\{\overline{(\frac{\partial u^1}{\partial x})^2} + \overline{(\frac{\partial u^1}{\partial y})^2} + \overline{(\frac{\partial u^1}{\partial z})^2} + \overline{(\frac{\partial v^1}{\partial x})^2} + \overline{(\frac{\partial v^1}{\partial y})^2} + \overline{(\frac{\partial v^1}{\partial z})^2} + \overline{(\frac{\partial w^1}{\partial x})^2} + \overline{(\frac{\partial w^1}{\partial y})^2} + \overline{(\frac{\partial w^1}{\partial z})^2}\} \tag{11}$$

The variables k and ϵ are modelled and related to the eddy viscosity ν_t by:

$$\nu_t = c_\mu \frac{k^2}{\epsilon} \tag{12}$$

in which:

y = lateral coordinate

v^1 = turbulent velocity in y-direction

ϵ = dissipation rate per unit mass

c_μ = turbulence constant

The transport equations for the kinetic energy (k) and its dissipation (ϵ) read (2-D):

$$\underbrace{\frac{\partial \overline{uk}}{\partial x} + \frac{\partial \overline{wk}}{\partial z}}_{\text{convection}} = \underbrace{\frac{\partial}{\partial x}\{\frac{\nu_t}{\sigma_k}\frac{\partial k}{\partial x}\} + \frac{\partial}{\partial z}\{\frac{\nu_t}{\sigma_k}\frac{\partial k}{\partial z}\}}_{\text{diffusion}} + \underbrace{\frac{\tau}{\rho}t,xx\frac{\partial \bar{u}}{\partial x} + \frac{\tau}{\rho}t,zx\frac{\partial \bar{u}}{\partial z} + \frac{\tau}{\rho}t,xz\frac{\partial \bar{w}}{\partial x} + \frac{\tau}{\rho}t,zz\frac{\partial \bar{w}}{\partial z}}_{\text{production}} - \epsilon \tag{13}$$

$$\underbrace{\frac{\partial \overline{u\epsilon}}{\partial x} + \frac{\partial \overline{w\epsilon}}{\partial z}}_{\text{convection}} = \underbrace{\frac{\partial}{\partial x}\{\frac{\nu_t}{\sigma_\epsilon}\frac{\partial \epsilon}{\partial x}\} + \frac{\partial}{\partial z}\{\frac{\nu_t}{\sigma_\epsilon}\frac{\partial \epsilon}{\partial z}\}}_{\text{diffusion}} - \underbrace{c_{2\epsilon}\frac{\epsilon^2}{k}}_{\text{destruction}} + \underbrace{c_{1\epsilon}\frac{\epsilon}{k}\{\frac{\tau}{\rho}t,xx\frac{\partial \bar{u}}{\partial x} + \frac{\tau}{\rho}t,zx\frac{\partial \bar{u}}{\partial z} + \frac{\tau}{\rho}t,xz\frac{\partial \bar{w}}{\partial x} + \frac{\tau}{\rho}t,zz\frac{\partial \bar{w}}{\partial z}\}}_{\text{production}} \tag{14}$$

in which c_{1_ϵ}, c_{2_ϵ}, σ_k, and σ_ϵ are empirical constants. Launder and Spalding (1974) recommend the following "standard" set of constants:

$c_\mu = 0.09$, $c_{1_\epsilon} = 1.44$, $c_{2_\epsilon} = 1.92$, $\sigma_k = 1.0$, $\sigma_\epsilon = 1.3$.

These values have been obtained by computer simulation of various types of free turbulent flows, but they can also be used for wall flows (Rodi 1980).
Assuming equal production and dissipation of the turbulence energy (k) in the near wall region, where a logarithmic velocity profile is supposed to apply and neglecting the convection of ϵ, the transport equation for ϵ (14) reduces to (Rodi 1980):

$$c_{1_\epsilon} = c_{2_\epsilon} - \frac{\kappa^2}{\sigma_\epsilon \sqrt{c_\mu}} \tag{15}$$

in which κ is the constant of Von Karman. Taking account of the above mentioned values of the turbulent constants the value of κ amounts 0.435. In the calculations a κ of 0.435 has been taken. Generally this constant is put on 0.40.
Equations (1), (2), (3), (12), (13), and (14) represent a set of six equations with six unknowns ($\bar{u}$, $\bar{w}$, $\bar{p}$, ν_t, k and ϵ) which can be solved numerically applying an appropriate set of boundary conditions.

It has already been mentioned that the transport equations of the kinetic energy (k) and the dissipation (ϵ) are strongly simplified. The exact equations are of no use in a turbulence model because new unknown correlations appear in the diffusion and dissipation terms. Equation (16) and (17) show the modelling of the diffusion terms in the transport equation of the turbulence energy in the x and z direction respectively.

x-direction:

$$\underbrace{\frac{\nu_t}{\sigma_k}\frac{\partial k}{\partial x}}_{a} = \underbrace{-\{\overline{u^1\frac{u^1u^1}{2} + u^1\frac{v^1v^1}{2} + u^1\frac{w^1w^1}{2}}\}}_{b} - \underbrace{\overline{u^1\frac{p^1}{\rho}}}_{c} +$$

$$\underbrace{\nu\{\overline{u^1[\frac{\partial u^1}{\partial x} + \frac{\partial u^1}{\partial x}]} + \overline{v^1[\frac{\partial v^1}{\partial x} + \frac{\partial u^1}{\partial y}]} + \overline{w^1[\frac{\partial w^1}{\partial x} + \frac{\partial u^1}{\partial z}]}\}}_{d} \tag{16}$$

z-direction:

$$\underbrace{\frac{\nu_t}{\sigma_k}\frac{\partial k}{\partial z}}_{a} = \underbrace{-\{\overline{w^1\frac{u^1u^1}{2} + w^1\frac{v^1v^1}{2} + w^1\frac{w^1w^1}{2}}\}}_{b} - \underbrace{\overline{w^1\frac{p^1}{\rho}}}_{c} +$$

$$\underbrace{\overline{\nu\{u^1[\frac{\partial u^1}{\partial z} + \frac{\partial w^1}{\partial x}] + v^1[\frac{\partial v^1}{\partial z} + \frac{\partial w^1}{\partial y}] + w^1[\frac{\partial w^1}{\partial z} + \frac{\partial w^1}{\partial z}]\}}}_{d} \qquad (17)$$

in which:

term a: modelled diffusive transport

term b: turbulent transport by velocity fluctuations

term c: turbulent transport by pressure fluctuations
[p^1 = fluid pressure fluctuation]

term d: turbulent transport by viscous shear stress fluctuations
(negligible)

The transport equation of the dissipation (ϵ) contains complex correlations, the behaviour of which is little known and for which fairly drastic model assumptions must be introduced in order to make the equation tractable. Especially the diffusion represents a combination of terms, which is not easy to model on theoretically grounds, (Hanjalic 1976).

2.2 Boundary conditions

The following types of boundary conditions are applied: bottom (log profile), free surface (rigid lid with free slip) inlet and outlet boundary.
In table 1 a distinction has been made with respect to the kind of boundary.

	momentum equations	k-ϵ equations
inflow boundary	$\bar{u}$ = given ; $\bar{w} = 0$	k and ϵ are given
outflow boundary	$\frac{\partial \bar{u}}{\partial x} = \frac{\partial \bar{w}}{\partial x} = 0$	$\frac{\partial k}{\partial x} = \frac{\partial \epsilon}{\partial x} = 0$
surface	$\frac{\partial \bar{u}}{\partial z} = 0$; $\bar{w} = 0$	$\frac{\partial k}{\partial z} = \frac{\partial \epsilon}{\partial z} = 0$
bottom	$\frac{\partial \bar{u}}{\partial z} = u_*/(\kappa z)$; $\bar{w} = 0$	$k = u_*^2/\sqrt{c_\mu}$; $\epsilon = u_*^3/(\kappa z)$

table 1 Boundary conditions [u_* = wall (bed) shear velocity]

The outlet boundaries are only applicable if the flow is in equilibrium (uniform flow). Then it is allowed to neglect the convective terms.
It has been assumed that at the surface the water depth does not change in the longitudinal direction (rigid lid approach). This is not fully correct because in reality the flow depth will increase somewhat in the deceleration region. Further assumptions, which have been made at the surface, such as a local minimum of the turbulence energy ($\frac{\partial k}{\partial z} = 0$) and a local maximum of the longitudinal velocity ($\frac{\partial \bar{u}}{\partial z} = 0$) are also not quite correct if an uniform flow will be considered. Measurements show that at the surface $\frac{\partial k}{\partial z}$ is not equal to zero (Nezu 1977). And if a logarithmic velocity profile is supposed to apply $\frac{\partial \bar{u}}{\partial z}$ can not be equal to zero here. Assuming a hydrostatic pressure distribution and a logarithmic velocity profile it follows that the eddy viscosity is parabolic (uniform flow). At the surface ν_t is then equal to zero. Substituting this value of the eddy viscosity into equation (12), it gives either k = 0 or the dissipation should tend to infinity. Both values for k and ϵ are not acceptable, because at the surface the turbulent velocities are not equal to zero (Nezu 1977) while the dissipation must tend to zero.
At the bottom, where a logarithmic velocity is supposed to apply, the vertical velocity component is zero and the longitudinal (tangential) is modelled by:

$$\frac{\partial \bar{u}_\tau}{\partial z} + \frac{u_*^2}{\nu_t} = 0 \qquad (18)$$

The determination of u_* in the k-ϵ-model has been realised by:

$$\bar{u}_\tau = \frac{u_*}{\kappa} \ln \frac{\delta_t}{z_o} \qquad (19)$$

a. smooth wall: $z_o = 0.11\nu/u_*$
b. rough wall: $z_o = 0.033k_s$

in which:
$\bar{u}_\tau$ = longitudinal (tangential) mean flow velocity
z_o = zero velocity level
k_s = equivalent roughness of Nikuradse
δ_t = distance from the wall beyond which the flow is completely turbulent

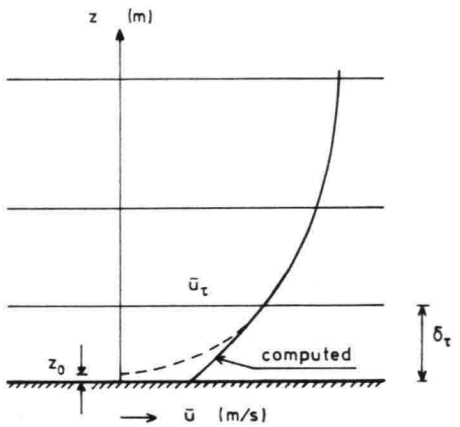

figure B Bottom modelling k-ϵ-model

See for a more detailed numerical description the computer program called ODYSSEE (k-ϵ-model) Delft Hydraulics 1987.

3.0 k-model

This model (Jorissen) has been developed to determine turbulence parameters after a sill. It was used to relate the relative turbulence and the length of the bottom-protection. This has been done for various ratios of the height of the sill and the water depth. In the model a depth-averaged turbulence ratio is defined as:

$$r_t = hu^1/q = c_k \int_0^h k(z)dz/q \tag{20}$$

in which:

r_t = depth-averaged turbulence
q = discharge per unit width
h = flow depth
c_k = empirical constant ($c_k = 1.0$)

The main differences between this model and the k-ϵ-model are the interactive relation between the velocity and the kinetic energy and, of course, the absence of the transport equation of the dissipation. In this k-model first the velocities are computed assuming a hydrostatic pressure distribution and a parabolic eddy viscosity.

continuity

$$\frac{\partial \bar{u}}{\partial x} + \frac{\partial \bar{w}}{\partial z} = 0 \tag{21}$$

motion

$$\overline{u\frac{\partial u}{\partial x}} + w\frac{\partial \bar{u}}{\partial z} = -\frac{\partial \bar{p}}{\rho \partial z} + \nu_t \frac{\partial^2 \bar{u}}{\partial z^2} \tag{22}$$

$$0 = -\frac{\partial \bar{p}}{\rho \partial z} + g \tag{23}$$

The eddy viscosity is computed by:

$$\nu_t = \kappa q\sqrt{g}/C(1 - z/h) \tag{24}$$

in which C represents the Chezy coefficient. Then the kinetic energy is computed by, see also equation (13) for the difference between the k-ϵ and k-model.

$$\overline{u\frac{\partial k}{\partial x}} = \nu_t\{\frac{\partial \bar{u}}{\partial z}\}^2 - \epsilon \qquad (25)$$

The dissipation ϵ is modelled by the expression (dimensional considerations):

$$\epsilon = \{c_d\ k^{3/2}\}/l_m \qquad (26)$$

in which:
c_d = empirical constant (c_d = 0.15)
l_m = mixing length (Prandtl) ; $l_m = \kappa z\sqrt{(1 - z/h)}$

The formulation of the eddy viscosity and the mixing length, which have been used in this model correspond with a uniform flow. After a sill or in a decelaration zone these assumptions are not correct, see figure 6. This model could be improved by adding equation (12). Then the model contains a set of 5 equations with 5 unknowns namely $\bar{u}$, $\bar{w}$, ν_t, k, ϵ.

4.0 Grid-generation

When a steady fluid flow passes a backward-facing step, a recirculation region will arise, having significantly higher levels of turbulence energy and stress than in the upstream or far-downstream regions. Although a recirculation does not always appear in the case of a local scour, the velocity profiles vary rapidly and so the mean-flow becomes highly dissipative there.
For this reason the grid distance is relatively smaller near the separation point and in the recirculation zone than elsewhere.
The layout of the grid network used in the calculation for the flow with the backward-facing step is shown in figure C.

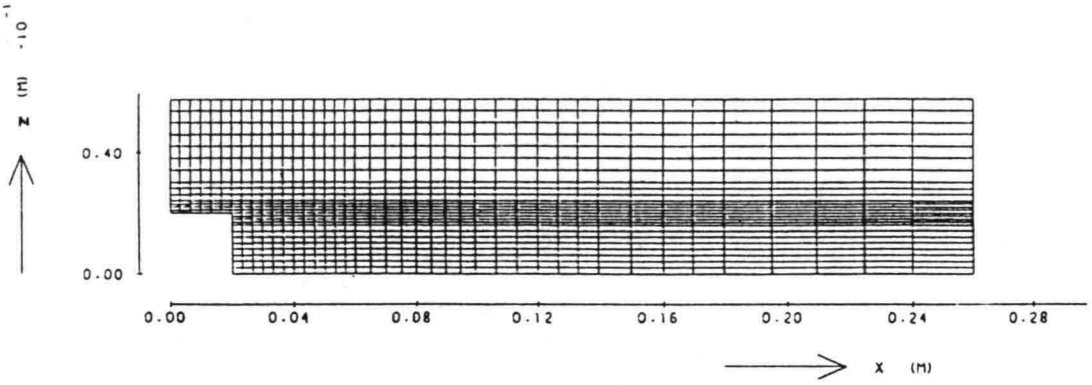

Figure C Calculation domain and partial layout of the grid network for backward-facing step (BS1)

This layout has been adopted from a sensitivity analysis carried out by Spalding and Launder (1974) who investigated a simular case. They showed, see table 2, the effect of six different grids on the turbulence distribution at a location 5.33 step heights behind the step and within the reciculation region. The first three columns show the effect of forward-step size while the last three show the effect of vertical grid size. The analysis shows that the 30 x 42 grid can be considered sufficiently refined.
This table is related to the configuration of a backward-facing step in which a total of 30 vertical stream grids are used to span 4.5 inches, out of which 14 nodes are used for the 1.5 inch step. The smallest

vertical grid spacing is 0.18 inch (=0.12 step height). In the longitudinal direction the smallest grid spacing is 0.3 inch. In this direction 42 nodes are used.

grid / z/H	20x30	20x42	20x47	25x42	30x42	36x42
	$k/\bar{u}_o^2 \times 10^2$					
0.18	2.201	2.210	2.216	2.229	2.244	2.248
0.30	2.795	2.840	2.850	2.855	2.860	2.863
0.51	3.608	3.617	3.622	3.637	3.669	3.672
0.63	3.942	3.949	3.953	3.958	3.961	3.964
0.75	3.968	3.978	3.985	3.996	4.005	4.058
0.87	3.686	3.762	3.770	3.864	3.898	3.910
0.95	3.255	3.513	3.520	3.591	3.602	3.606
1.065	2.641	2.708	2.716	2.726	2.744	2.747
1.125	1.988	2.116	2.121	2.130	2.139	2.139

table 2 Effect of grid size on the turbulence kinetic energy, $k/\bar{u}_o^2$ (Spalding and Launder 1974).

Based on approximately 1200 nodes a grid has been generated for two backward-facing steps and three local scour holes.

	grid	h_{max}	
backward-facing step 1	28 x 42	0.058 m	rectangular
backward-facing step 2	28 x 56	0.45 m	rectangular
local scour hole 1	15 x 66	0.37 m	curved
local scour hole 2	15 x 76	0.45 m	curved
local scour hole 3	15 x 79	0.60 m	curved

Table 3 Grid generation

Launder and Spalding made their calculations with a numerical model called PHOENICS, whereas the calculations in this project were made with the model ODYSSEE. It is possible that these models do not yield exactly the same results. Regarding the differences between the configuration of a backward-facing step (rectangular grid) and a local scour (curved grid), it is recommended to make a grid refinement study for a local scour.

5.0 Applications

5.1 Backward-facing step 1

Nezu et al (1987) carried out turbulence measurements of a backward-facing step flow, including the reverse flow region in an open channel with the aid of a two component Laser Doppler anemometer. The mean velocity distribution and turbulence characteristics were obtained. The experiments were conducted in a 8 m. long, 30 cm. wide and 20 cm. deep tilting flume. The backward-facing step with a height H = 2 cm. was located at a distance of 6.8 m. downstream from the channel entrance. The channel bed was flat and smooth. The Froude number of the flow was no more than Fr = 0.19 yielding a small variation of the free surface. The most important hydraulic data of this experiment were:

h	$= 0.058$ m	; flow depth (downstream)
H	$= 0.020$ m	; step height
$\bar{u}_{s,o}$	$= 0.243$ m/s	; mean surface velocity at initial section
$\bar{u}$	$= q/h = 0.142$ m/s	; depth-averaged velocity (downstream)
Re	$= h\,\bar{u}/\nu = 8200$	; Reynolds number
Fr	$= \bar{u}/\sqrt{(gh)} = 0.19$	; Froude number
x_R/H	$= 6.3$	; x_R = reattachment length

Table 4 Hydraulic data (BS 1)

5.1.1 Mean flow velocity

Figure 1 shows measured and computed k-ϵ-model profiles of the mean velocity $\bar{u}$. The mean velocity obeys the log-law distribution upstream of the step ($x<0$). Immediately downstream of the step, a shear layer is generated. A reverse flow occurs near the bed up to the reattachment point (x_R). Downstream of x_R, a new sub-boundary layer is formed, see figure D.

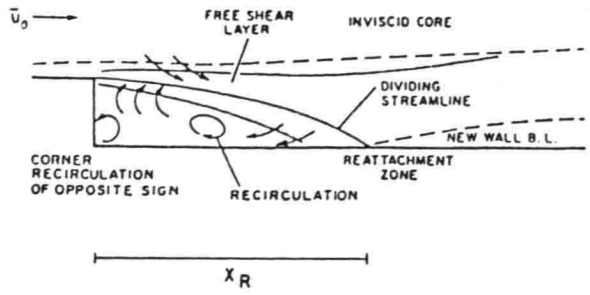

Figure D Typical plot of a backward-facing flow

For x = H (H = step height) the following remarks can be made.

1. The point of zero mean velocity of the computed velocity profile is closer to the bottom than the measured one.
2. The computed circulated discharge is relatively bigger.

It has to be noted that for $7H < x < 10H$ the computed velocities near the bottom are somewhat larger than the measured ones.
The profiles have also been computed by the profile method (see Van Rijn 1987, Hoffmans 1987). They differ more from the measurements (LDA) than the values comptuted by the k-ϵ-model, especially in the recirculation region. Although this method is not based on the hydronamic equations its simplicity could be a big advantage provided the calculated results are correct.

5.1.2 Kinetic energy

Figure 2 shows the computed and measured profiles of the kinetic energy for several verticals. The solid curves have been computed by the k-ϵ-model, whereas the other two curves have been determined by the measurements. The lateral (y-direction) fluctuating velocity (v^1) namely, is unknown, because the measurements were only carried out in the x and z direction. The lower limit of the kinetic energy is equal to:

$k = \frac{1}{2}\{\overline{(u^1)^2} + \overline{(w^1)^2}\}$ setting $v^1 = 0$, and the upper limit

$k = \frac{3}{4}\{\overline{(u^1)^2} + \overline{(w^1)^2}\}$ assuming that $\overline{(v^1)^2} = \{\overline{(u^1)^2} + \overline{(w^1)^2}\}/2$

For an equilibrium flow this is an upper limit because the lateral velocity fluctuation is smaller than the longutudinal (u^1) and the vertical (w^1) component, respectively. The measured kinetic energy will lie between these two boundaries.
Comparing measurements and calculations the overall agreement is quite reasonable. The differences mainly apply in the recirculation zone near the bottom. Here the computed kinetic energy is somewhat larger than the k which follows from the measured values. Probably this is owing to the coefficient c_μ.
For equilibrium shear layers, where the production (P) is equal to the dissipation (ϵ), the equations (12) and (13) can be combined to:

$$c_\mu = \{u_*^2/k_{wall}\}^2 = \{\tau_o/\rho k_{wall}\}^2 \qquad (27)$$

in which τ_o represents the bed shear stress. The value of $c_\mu = 0.09$ was chosen on the basis of experiments in uniform flows in which P and ϵ were in approximate balance. For far-field jets and wakes where the cross-velocities differ with respect to the longitudinal velocities ($\approx$ free stream velocity), P is significantly different from ϵ and then c_μ was found to be different from the standard value. The range of applicability of the k-ϵ-model can be extented when some of the constants in the k-ϵ-model are replaced by functions of suitable flow parameters. Rodi introduced a function for an axisymmetric jet.

$$c_\mu = 0.09 - 0.04f \qquad (28)$$
$$c_{2\epsilon} = 1.92 - 0.0667f \qquad (29)$$
$$f = f(\delta, \bar{u}, x) \qquad (30)$$

in which δ is the distance from the symmetry axis to the 1% point at the outeredge.
Figure 3 shows some profiles of the kinetic energy in a trench for $c_\mu = 0.09$ and 0.20. For the larger value of c_μ the kinetic energy decreases over the entire vertical. Near the wall the agreement between measurements and calculations ($c_\mu = 0.20$) is better. However in the region $0.1h < z < h$ they deviate more from the measurements than the standard values computed with the standard value of c_μ.

According to Van Rijn (1983) the influence of a larger value of c_μ on the computed mean flow velocity, shear stress and eddy viscosity profiles was negligible small.

5.1.3 Wall (bed) shear velocity

The wall shear stress (τ_o) is an important quantity as it will determine the sedimenttransport.
Figure 4 shows the wall-shear-stress coefficient (c_f) which is defined as:

$$c_f = 2(u_*/\bar{u}_{s,o}) \tag{31}$$

Nezu obtained u_* from van Driest's curve, as shown in figure E.

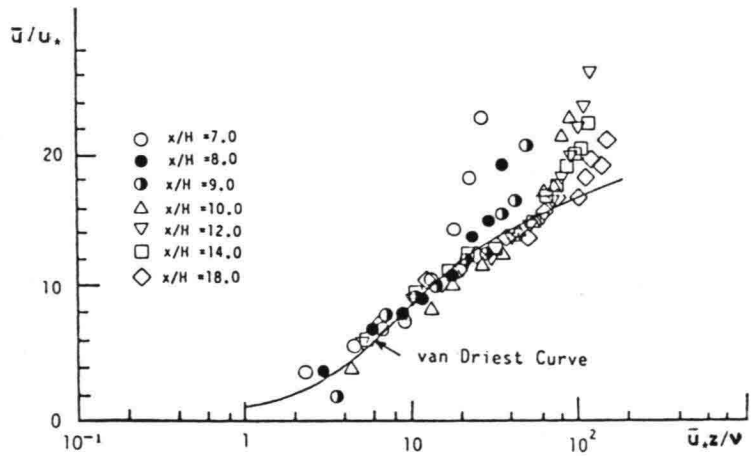

Figure E Velocity distribution near the wall downstream of the reattachment (Nezu 1987)

For a comparison, figure 4, replots several computed curves and also experimental values which were obtained in boundary layers. One was calculated by using the following formula which Ludwieg and Tillmann (1949) obtained experimentally in boundary layers.

$$c_f = 0.256.10^{-0.678\delta/\theta}.\{\bar{u}_{s,o}\theta/\nu\}^{-0.268} \tag{32}$$

in which:
δ = displacement thickness
θ = momentum thickness
For a definition of the displacement and momentum thickness, see E appendix A.

In figure 4 the dotted line shows the k-ϵ predictions. It should be noted that the calculated values of c_f by the k-ϵ-model coincide well with the experimental values and the calculated curve from equation 32.

5.1.4 Reynolds stresses

Figure 5 shows computed and measured Reynolds stresses for various verticals (H, 4H, 7H, 10H). Because the k-ϵ-model does not reproduce the Reynolds stresses directly, these values have been computed as follows: The shear-stress is defined as:

$$\tau_{t,zx} = \rho\nu_t\{\frac{\partial\bar{u}}{\partial z} + \frac{\partial\bar{w}}{\partial x}\} = -\rho\overline{u'w'} \qquad (33)$$

in which the left term (middle) represents the computed shear stress and the most right term the measured one.

Assuming $\frac{\partial\bar{w}}{\partial z} \ll \frac{\partial\bar{u}}{\partial z}$ equation (33) simplifies into:

$$\nu_t \frac{\partial u}{\partial z} = \overline{u'w'} \qquad (34)$$

In the deceleration zone with back flow it is striking that the computed values agree well with the measured ones. More downstream, 5H < x < 10H, the agreement is less spectacular at the height of the threshold, (z = H). There the measured Reynolds (τ_{zx}) is smaller than the calculated one. As the measured and calculated flow profile were almost identical this implies that the eddy viscosity derived from the measurements is smaller than the calculated one. Since the eddy viscosity will be correlated to the diffusive transport of sediment (suspended) this might have consequences for the calculation of sediment transport. Overall, the computed reproduction of the mixing layer is very good.

5.2 Backward-facing step 2

This k-ϵ calculation has been made to form a link between the computation of the first backward-facing step and those of the local scours. The differences between the first and second backward-facing calculation are:

1. larger Reynolds number
2. smaller Froude number
3. relative greater calculation domain in horizontal direction

	Backward-facing step		
	BS1	BS2	
h (downstream)	0.058	0.45	(m)
H	0.02	0.15	(m)
$\bar{u} = q/h$	0.142	0.269	(m/s)
$Re = h\,\bar{u}/\nu$	8200	121000	(-)
$Fr = \bar{u}/(gh)$	0.19	0.13	(-)
x_R/H	5.2	4.8	(-)
	6.3 (= measured)		

Table 5 Hydraulic data (BS1 and BS2)

5.2.1 Results (k-ϵ-model)

The figures 7, 8, 9, 10 and 11 show some results of the k-ϵ computation of the second backward facing step.
From figure F it can be seen that the computed reattachment length (x_R/H=4.8) is too small, this is probably owing to the empirical constants in the k-ϵ-model, see also 5.1.2.

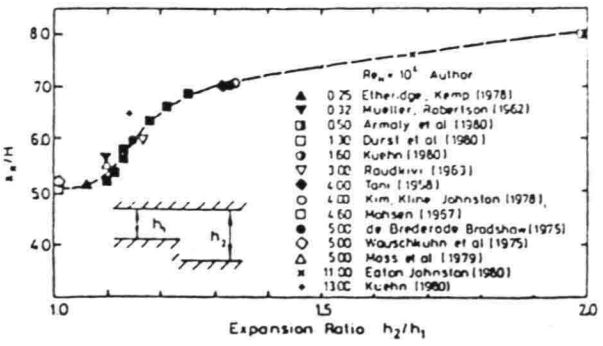

Figure F Dependence of separation region lenght on expansion ratio (AGARD 1985)

After the recirculation zone where a new sub-layer will be developed, it is not very clear from the velocity profiles where an equilibrium flow occurs, see e.g the verticals at 40H (x = 6.3 m) and 60H (x = 9.3 m). Directly after the threshold the kinetic energy is strongly growing. It reaches its maximum approximately at x = 7H (x = 1.2 m). Then the average kinetic energy is decreasing, see figure 12.
The computed wall shear stress (k-ϵ), see figure 11, for a nearly uniform flow is approximately 8% larger than the computed values by the roughness formulas of Darcy-Weisbach and White Colebrook respectively.

Darcy-Weisbach: $f = 0.24/\{\log^2 1.3Re\sqrt{f})\}$ (35)

White Colebrook: $C = 18\ \log\{12h/(0.11\nu/u_*)/3.5\}$ (36)

in which f is a roughness parameter, $f = 8(u_*/\bar{u})^2$.

Both formula calculate a wall shear velocity which are equal to 0.0109 - 0.0110 m/s (f = 0.0132 and C = 76.6 $m^{1/2}$ / s) respectively, whereas the k-ϵ-model predicts a value of 0.0121 m/s. Figure 4 already showed that the computed (k-ϵ) friction coefficient (c_f) was somewhat larger than the experimental values (Nezu 1987) and the computed values by the Ludwieg-Tillmann's formula.

5.2.2 Results k-model (averaged k)

Figure 12 shows the computed averaged kinetic energy after a threshold as a function of the longitudinal distance. The function starts directly with a maximum and decreases to an equilibrium value (uniform flow).
In the recirculation zone the mean values of the k-model are larger than the k-ϵ results. Apparently the k-model generates in the centre-line in the mixing layer after the threshold larger values of k. With increasing length these values become smaller than those obtained by the k-ϵ-model. Probably this is owing to the neglect of the diffusion terms in the k-model.
Figure G shows the influence of the diffusion of the kinetic energy after a threshold. Especially in the outside region (at the top) the transport by the velocity fluctuations gives an important contribution to the kinetic energy.

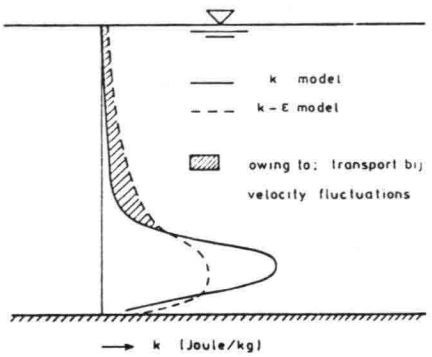

Figure G Kinetic energy distribution after a threshold

5.3 Local scours

5.3.1 General

Measurements in local scours were carried out by Delft Hydraulics (Breusers). The longitudinal velocity component was measured by a micro-propellor. This instrument is less accurate than a Laser Doppler anemometer. The measurement range of a micro-propellor depends mainly on the type of propeller. On the average the measurement range is from 0.025 to 10.0 m/s. This means that it is not possible to measure negative velocities.

The slope of the local scour directly after the armour layer was approximately 1:4.5 for all three scours. Probably it was not steep enough to create a reverse flow; the measurements as well as the calculations of the k-ϵ-model indicate mean positive velocities near the bottom.
The most important hydraulic data of these experiments were:

	Local scour			
	LS1	LS2	LS3	
h_o	0.30	0.30	0.30	(m)
h_{max}	0.38	0.45	0.59	(m)
$\bar{u}_o = q/h_o$ (k-ϵ)	0.332	0.396	0.345	(m/s)
$\bar{u}_{s,o}$ (k-ϵ)	0.410	0.483	0.433	(m/s)
k_s (upstream)	0.02-0.03	0.02-0.03	0.02-0.03	(m)
k_s (downstream)	0.0005	0.0005	0.0005	(m)
$Re = \bar{u}_o h_o/\nu$	99600	118900	103500	(-)
$Fr = \bar{u}_o/\sqrt{(gh_o)}$	0.19	0.23	0.20	(-)

table 6 Hydraulic data (local scours)

5.3.2 Mean flow velocities

The figures 12, 13 and 14 show several computed and measured velocity profiles for local scour 1, 2 and 3, respectively.
At first it can be noted that the computed (k-ϵ) bottom velocities are too large. This has already been discussed in 5.2. In general the agreement between the measured and calculated velocities is fairly well. In the case of local scour 2 it seems that the values computed by the k-ϵ-model are not well predicted especially in the verticals 3, 5, 9 and 10. However, part of the differences appear to be attributed to an error in the velocity measurements. Integrating the measured velocity profiles of the sections above mentioned yields the following discharges $q_3 = 0.106\ m^2/s$, $q_5 = 0.105\ m^2/s$, $q_9 = 0.105\ m^2/s$, $q_{10} = 0.104\ m^2/s$, whereas the discharge at the initial section is $0.118\ m^2/s$. This means a difference of $0.013\ m^2/s$ ($\approx 12\%$).

5.3.3 Turbulence parameters

The figures 16 through 24 show turbulence predictions by the k-ϵ-model for the three scours.
At the initial section the k has to be given in the k-ϵ-model as a boundary condition. A good approach is setting k to $(u^1)^2$, so that the calculated value is an average of a lower limit [$k = 0.5(u^1)^2$] and an upper limit [$k = 1.5(u^1)^2$]. Figure 16 shows that at section 1 the calculated k near the bottom does not agree with the measurements. At section 4 and further downstream the calculated values of k are greater over the entire vertical than the measured ones. The same story applies figure 17; showing also larger calculated values of k.
At the inflow boundary of local scour 3, figure 18, the given k was not set on the average of a lower and upper limit but was made equal to the upper limit in order to examine the effect of the initial turbulence on the local scour in both cases. The differences appear to be negligible.
In figure 19, 20 and 21 the influence from the rough bottom upstream and the smooth one downstream on the near-bottom velocities is very clear.
The initial profile of the dissipation in figure 21 (local scour 3) differs from the beginning profiles of local scour 1 and 2. This is owing to the difference in the given turbulent kinetic energy at the initial section. If the eddy viscosity distribution is the same for all three scours this is easy to verify with equation (12).
At the inlet-boundary the eddy viscosity profiles are modelled as follows; parabolic in the lower half of the depth and a constant value in the upper half of the depth. This approach has been adopted by van Rijn (1984). The difference between this method and a parabolic eddy viscosity distribution is small for the velocities in the outer region, see figure 13, 14 and 15.

6.0 Conclusions and recommendations

The k-ϵ-model predicts the velocities fairly well. The computed turbulence profiles, however, are less satisfactory if compared with measurements. At this moment there are no models which can calculate the above mentioned parameters in a better way. A disadvantage of the k-ϵ-model is the relatively large computation time needed to solve the complete set of equations, see 2.1. Therefore, the k-ϵ-model is not a very attractive model for long-term morphological computations and a simpler model will be required, such as

DUCT-model	[Vreugdenhil]
PROFILE-model	[van Rijn]
k-model	[Jorissen]

However, each of them has its own shortcomings. Further research is necessary to determine which model is most suitable to predict the velocity field, the shear stresses and the viscosity profiles in view of costs and reliability. The k-ϵ-model can serve as a reference to determine this choice.

References

Booy, R., 1986,
Turbulentie in de waterloopkunde,
Technische Universiteit Delft, Civiele Techniek.

Delft Hydraulics, Delft 1987,
Documentation to the computerprogram ODYSSEE, part 3^{b}: Mathematical and numerical description of the code Ulysse, 2^{e} version.

Hanjalic, K. and Launder, B.E., 1976,
Contribution towards a Reynolds-stress closure for low-Reynolds number turbulence, Journal of fluid mechanics, volume 74, part 4, pp. 593-610.

Hinze, J.O., 1975,
Turbulence, second edition,
Mc. Graw Hill Book Co., New York.

Hoffmans, G.J.C.M., 1987,
Analyse geparametriseerd waterbewegingsmodel 'Profielenmethode',
Technische Universiteit Delft, Civiele Techniek, rapport no. 1-88.

Jorissen, R.E., 1987,
Numeriek model ter bepaling van de ontwikkeling van snelheids- en turbulentie verticalen achter een drempel,
Technische Universiteit Delft, Civiele Techniek.

Kay, J.M. and Nedderman R.M., 1985,
Fluid mechanics and transfer processes,
Cambridge University Press.

Launder, B.E. and Spalding, D.B., 1974,
Numerical computation of turbulent flows, Computer methods in applied mechanics and engineering, vol 3, pp. 269-89.

Ludwieg, H. and Tillmann, W., 1949,
Untersuchungen uber die Wandschubspannung in Turbulenten Reibungsschichten, Z. Angew. Math. Mech., Bd 29, no. 1/2, pp. 15-16.

References (continued)

Nakagawa, H. and Nezu, J., 1987,
Experimental investigation on turbulent structure of backward-facing step flow in an open channel, Journal of Hydraulic Research, Vol 25, no 1, pp. 67-88.

Nezu, J., 1977,
Turbulent structure in open channel flows, (translation of doctoral dissertation published in japanese),
Department of Civil Engineering, Kyoto University, Kyoto 606, Japan.

Rijn, L.C. van, 1983,
Siltation in dredged trenches, two dimensional mathematical flow model with a two equation turbulence closure,
Report S488 part 1, Delft Hydraulics.

Rijn, L.C. van, 1984,
Sediment transport, part 2: Suspended load transport, Journal of Hydraulic Engineering, Vol. 110, no. 11, pp. 1613-1641.

Rijn, L.C van, 1987,
Mathematical modelling of morphological processes in the case of suspended sediment transport, PhD Thesis,
Delft University of Technology, Department of Civil Engineering.

Rodi, W., 1980,
Turbulence models and their application in hydraulics,
IAHR-section on fundamentals of division 2, Delft.

Simpson, R.L., 1985,
Two-dimensional turbulent separated flow,
AGARDograph no. 287, Vol 1.

Wijngaarden, N. van, 1984,
Fundamenteel onderzoek naar voorspellen van ontgrondingen,
Waterloopkundig Laboratorium Delft, rapport M1820.

Appendix A

Definition of boundary-layer thickness

A quantity known as the displacement thickness δ^* can be defined as follows. Referring to figure A1, the volume flow is given by:

$$q = \int_0^{\delta} \bar{u} dz = \bar{u}_1(\delta - \delta^*) \tag{A1}$$

i.e.

$$\delta^* = \int_0^{\delta} (1 - \bar{u}/\bar{u}_1) dz \tag{A2}$$

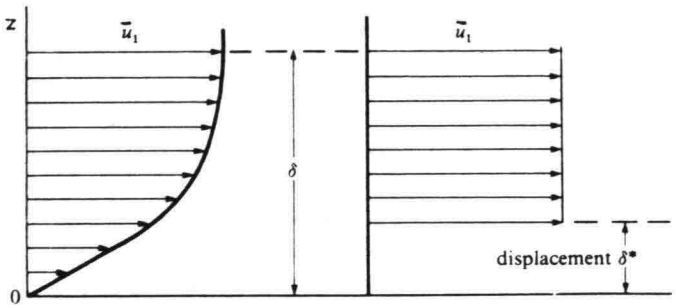

Figure A1 Displacement thickness

The physical meaning of this definition is that δ^* represents the distance by which an equivalent uniform stream would have to be displaced from the surface as indicated in figure A1 to give the same total volume flow. A similar picture may be drawn for the momentum flow in the boundary layer. Referring to figure A2, the momentum flow (M) in the boundary layer is given by:

$$M = \int_0^{\delta} \rho \bar{u}^2 dz = \rho \bar{u}_1^2 (\delta - \delta^{**}) \tag{A3}$$

and assuming constant density, equation (A3) reduces to:

$$\delta^{**} = \int_0^{\delta} (1 - \bar{u}^2/\bar{u}_1^2) dz \tag{A4}$$

The momentum thickness or the momentum-displacement thickness θ as indicated in figure A2 is defined by $\theta = \delta^{**} - \delta^{*}$. From (A2) and (A3) θ takes the form:

$$\theta = \delta^{**} - \delta^{*} = \int_0^{\delta} \bar{u}/\bar{u}_1(1 - \bar{u}/\bar{u}_1)dz \qquad (A5)$$

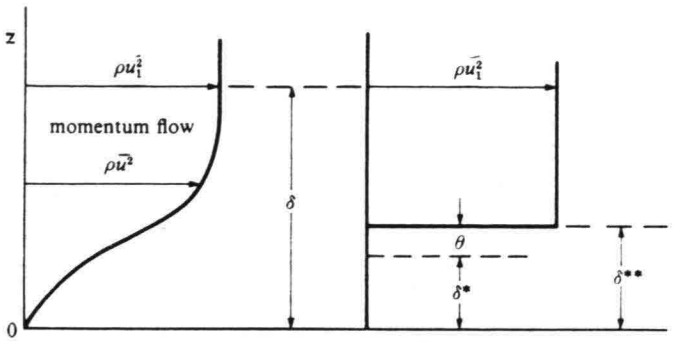

Figure A2 Momentum displacement

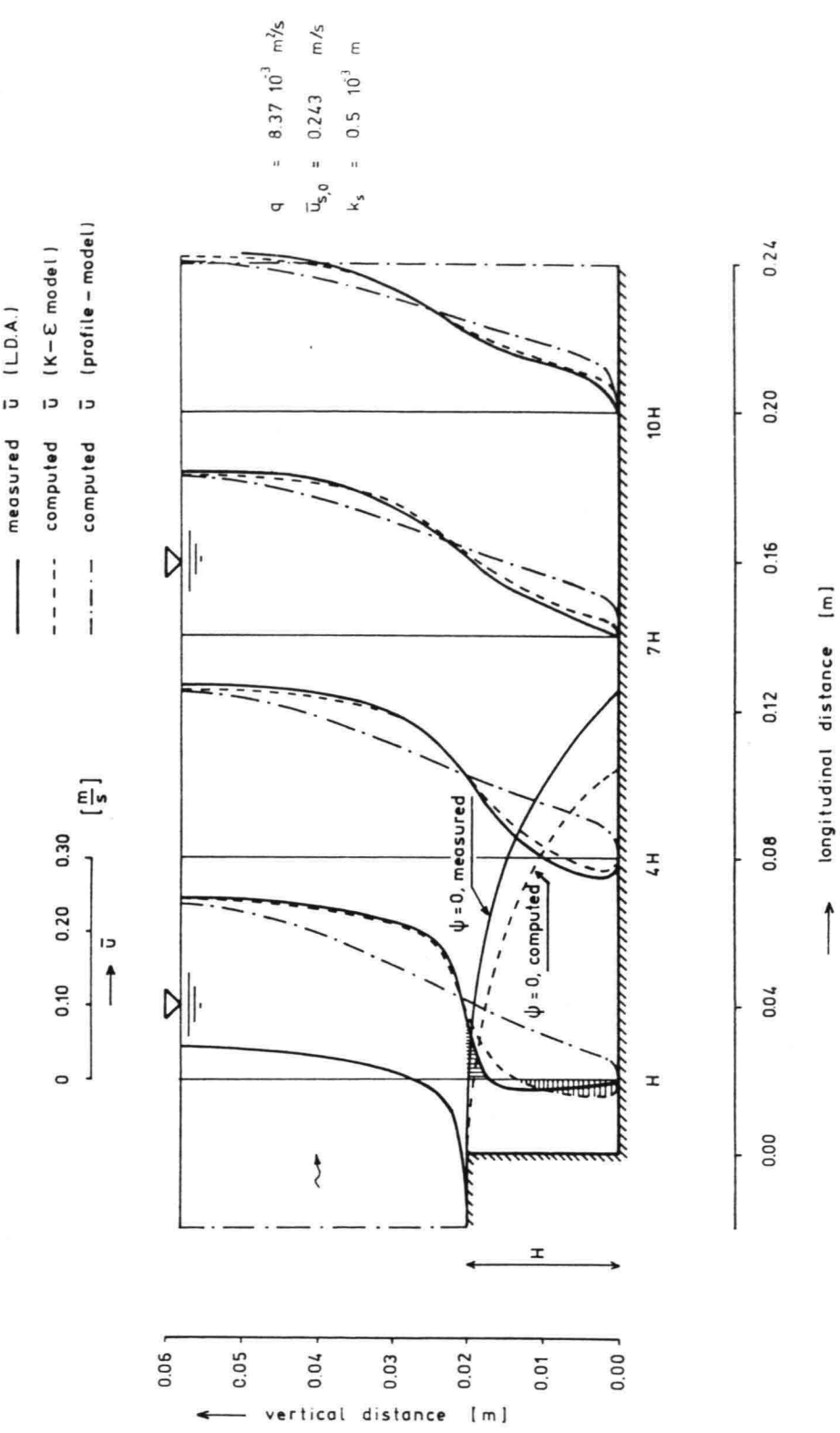

figure 1 Mean flow velocity profiles

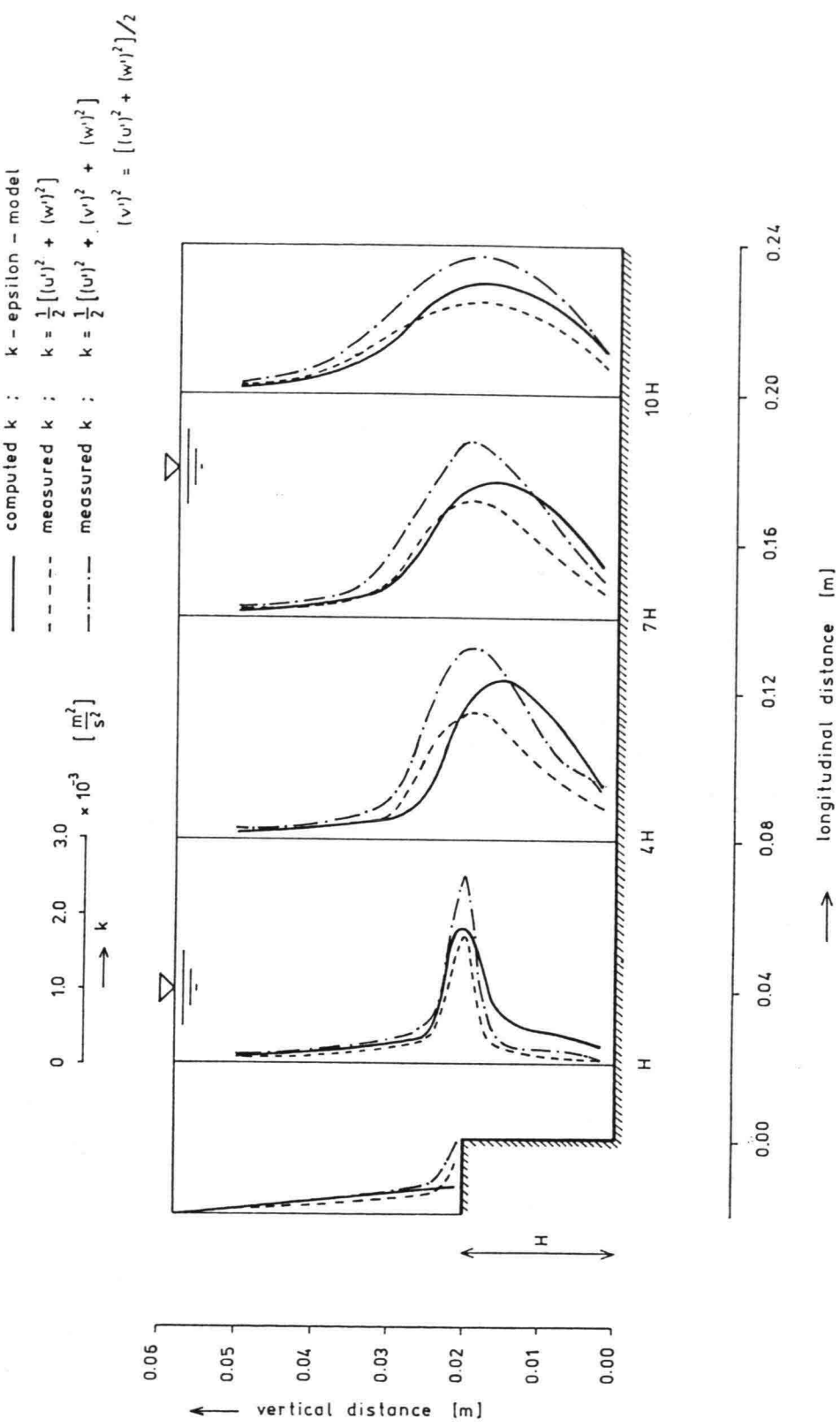

figure 2 Kinetic energy profiles (per unit mass)

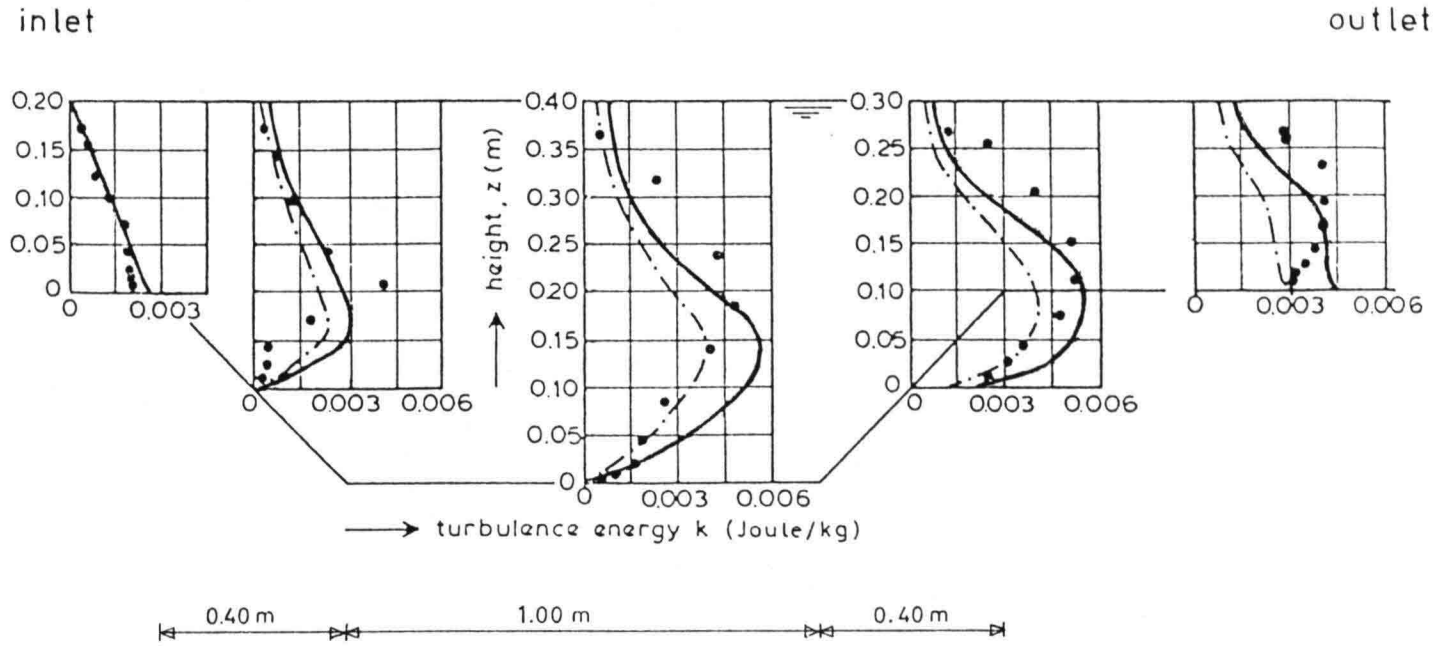

	C_μ	$C_{1\varepsilon}$	K
———	0.09	1.65	0.4
—·—	0.20	1.51	0.4

$C_{2\varepsilon}$, σ_k, σ_ε standard values

• measurements

figure 3. Turbulence energy profiles [van Rijn 1983]

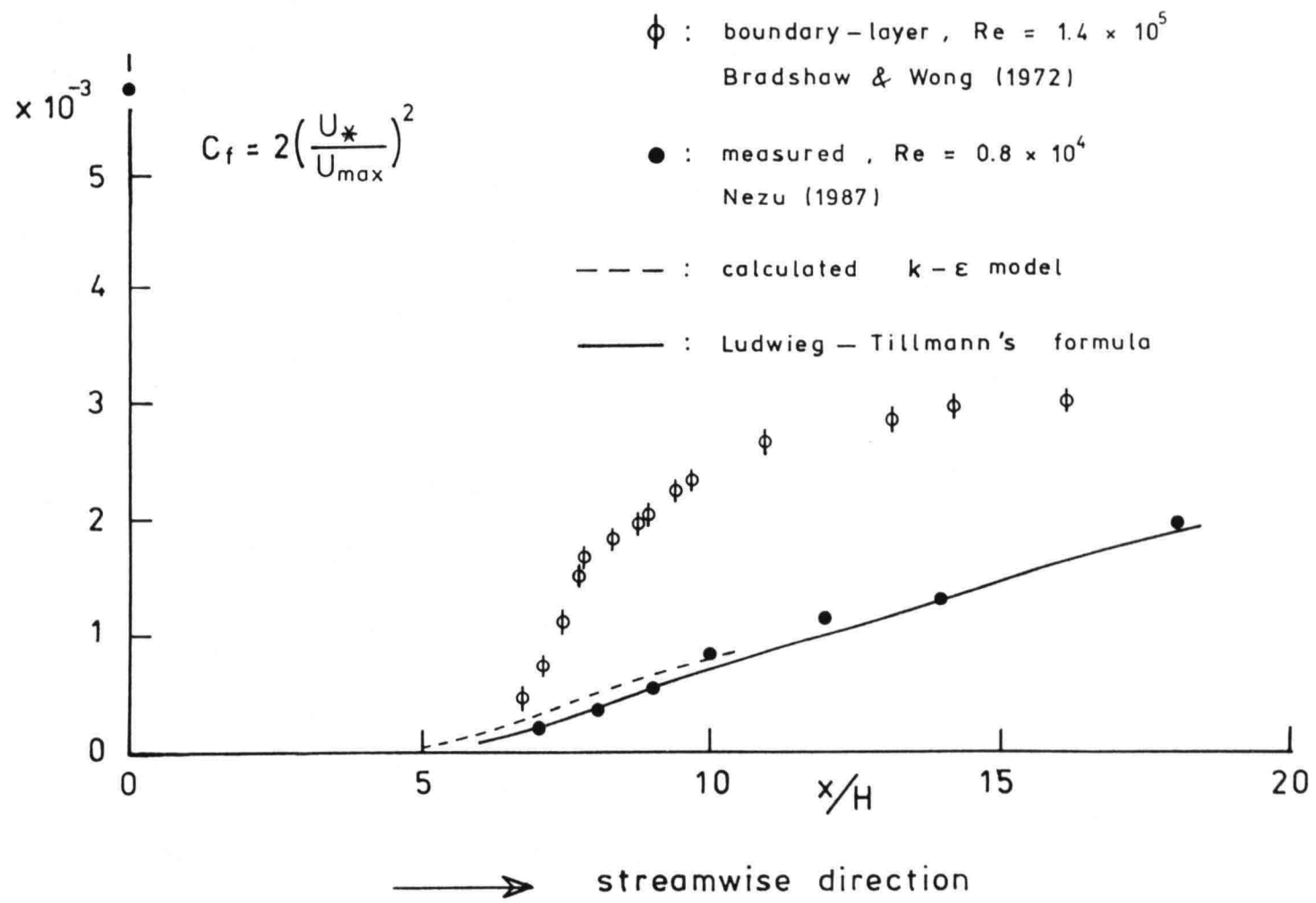

figure 4. Wall-shear stress coefficient (BS 1)

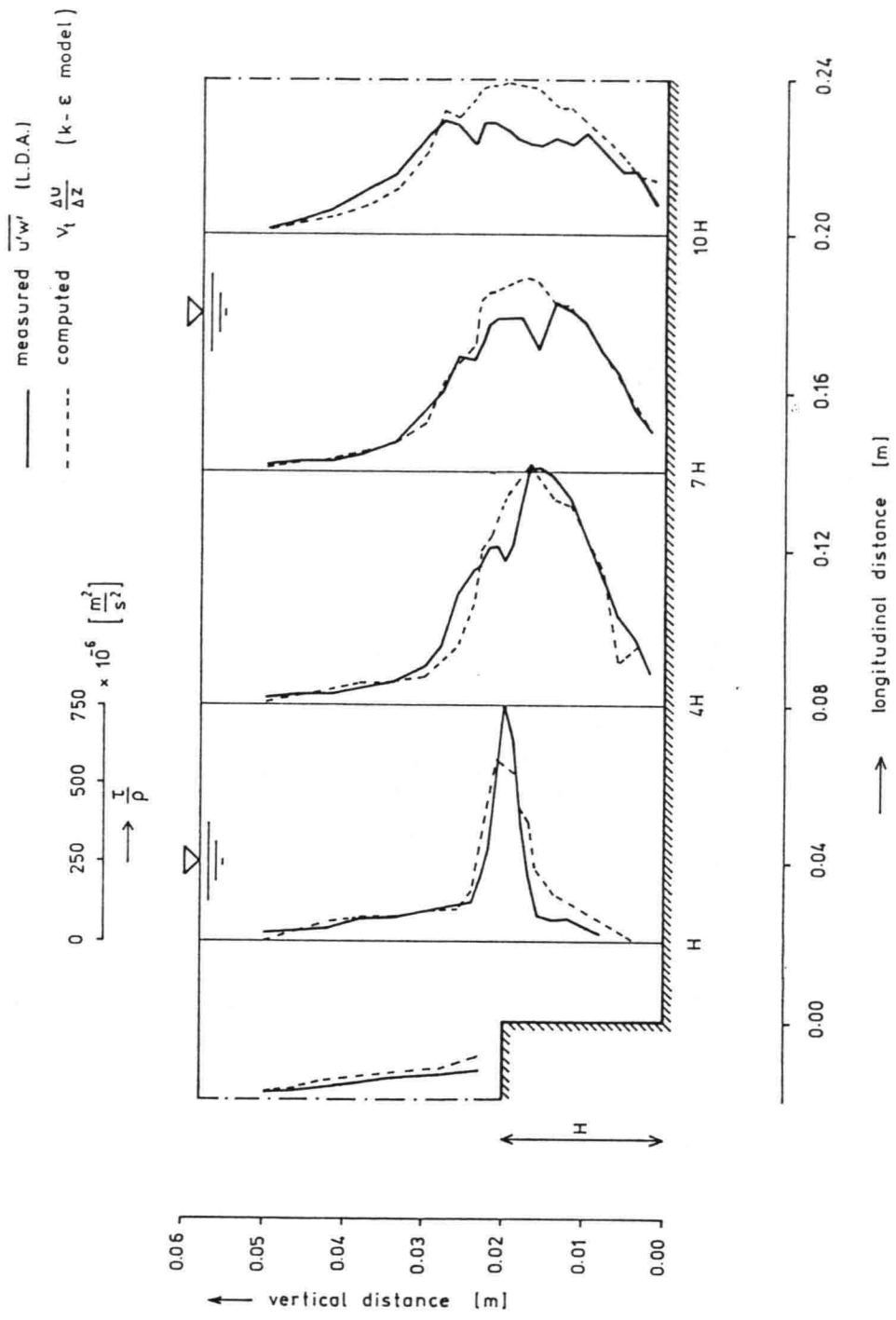

figure 5 Reynolds stress profiles

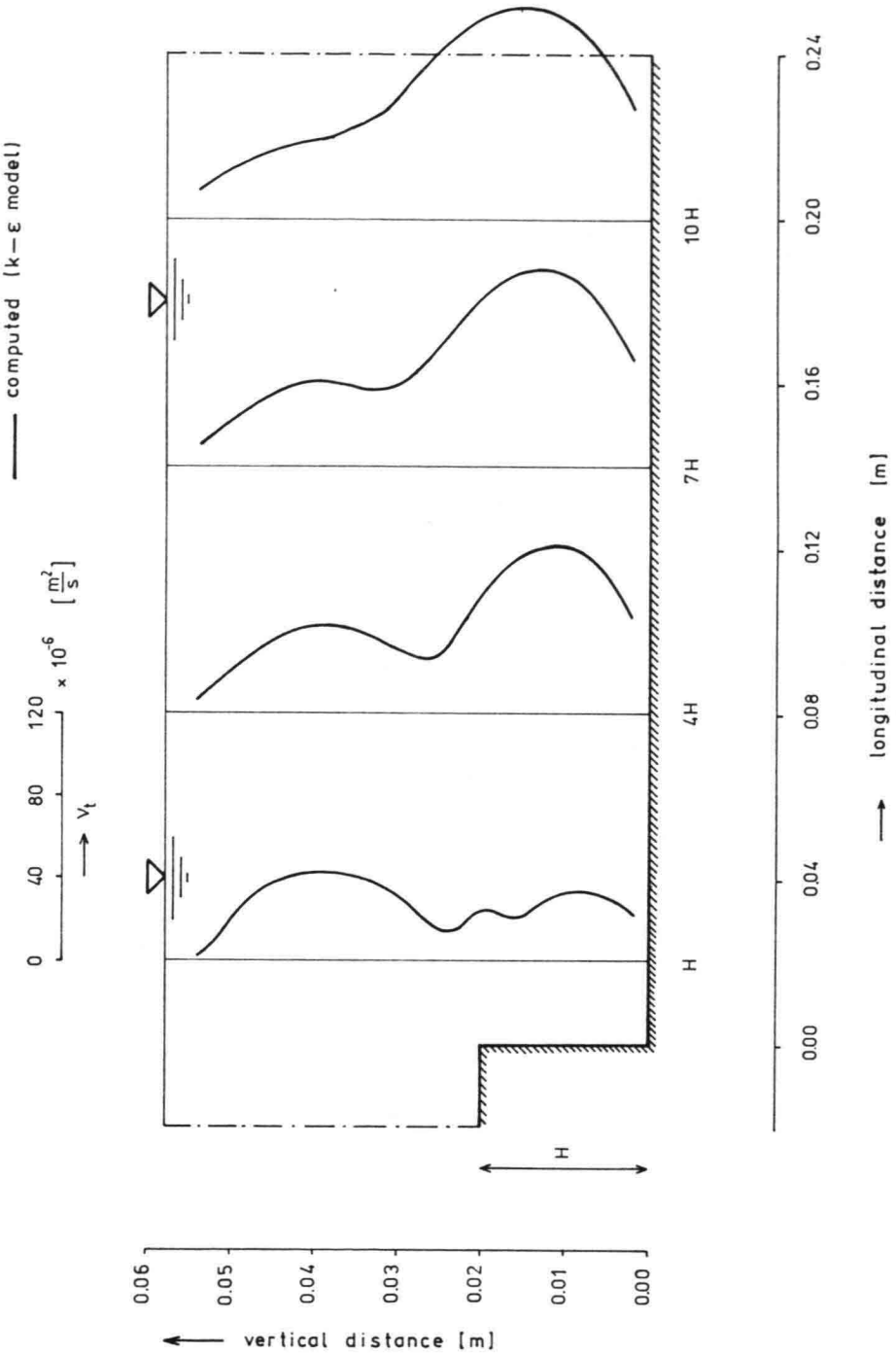

figure 6 Eddy viscosity profiles

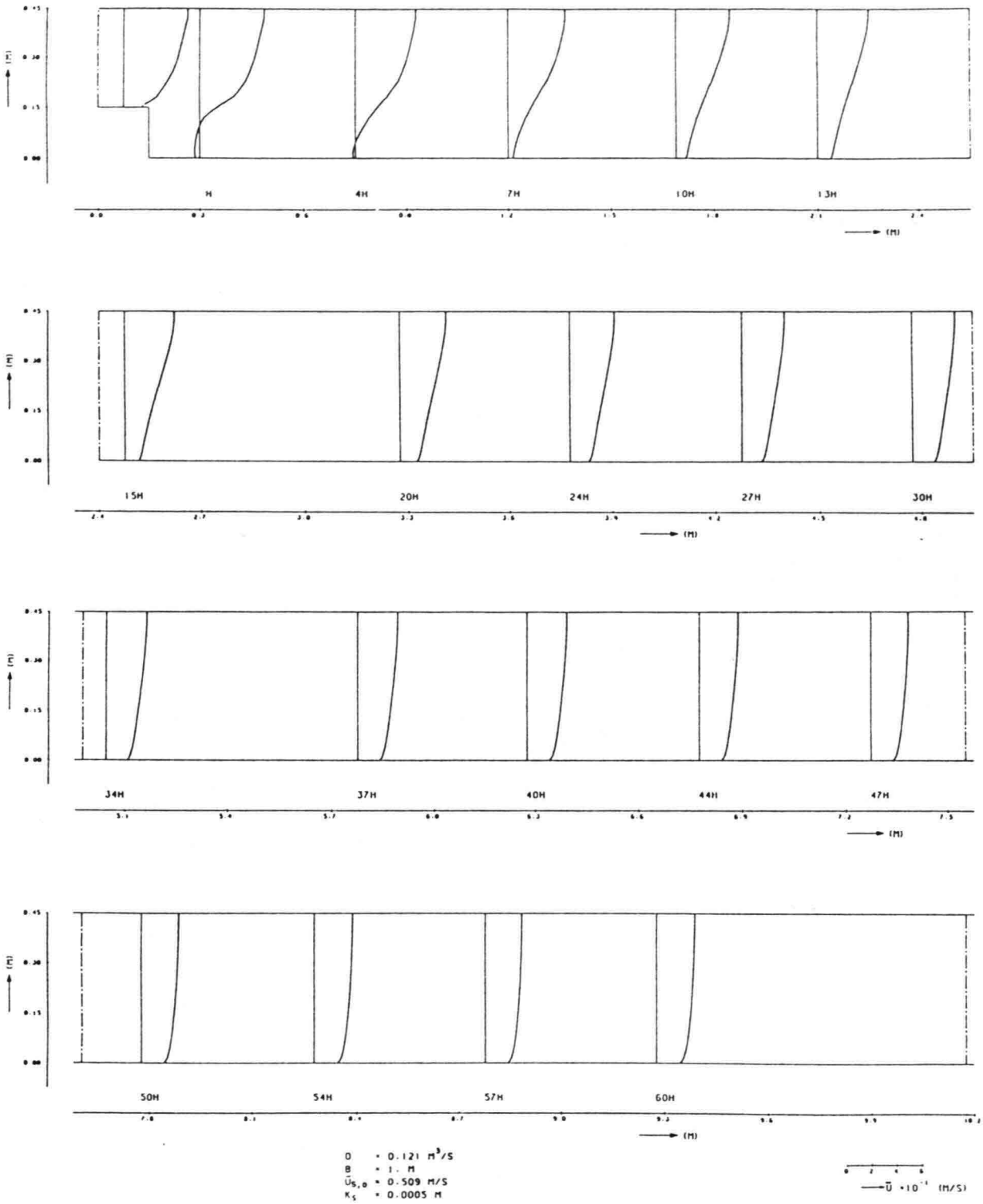

figure 7. Mean flow velocity profiles ($k-\varepsilon$ predictions)

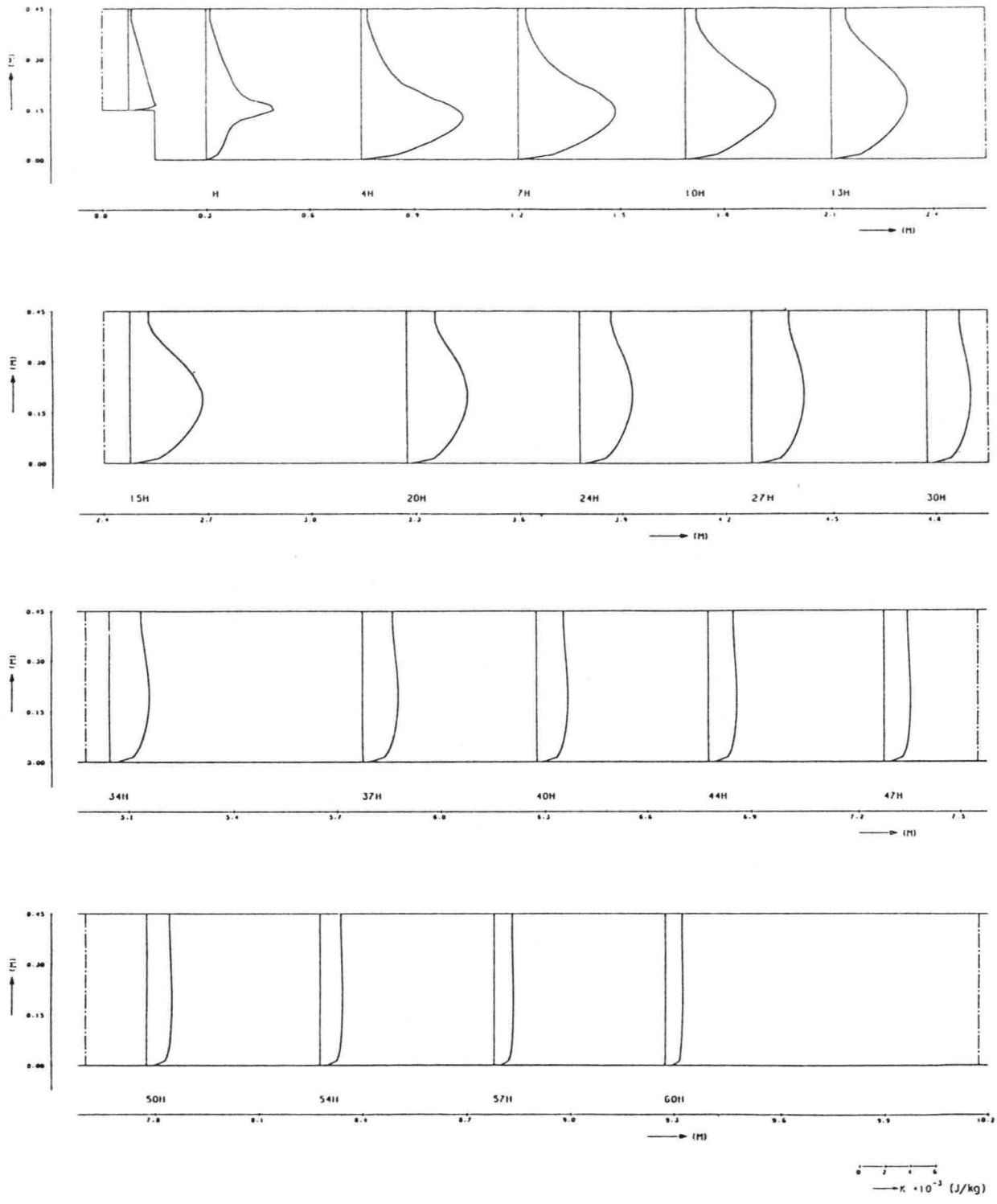

figure 8. Kinetic energy profiles ($k-\varepsilon$ predictions)

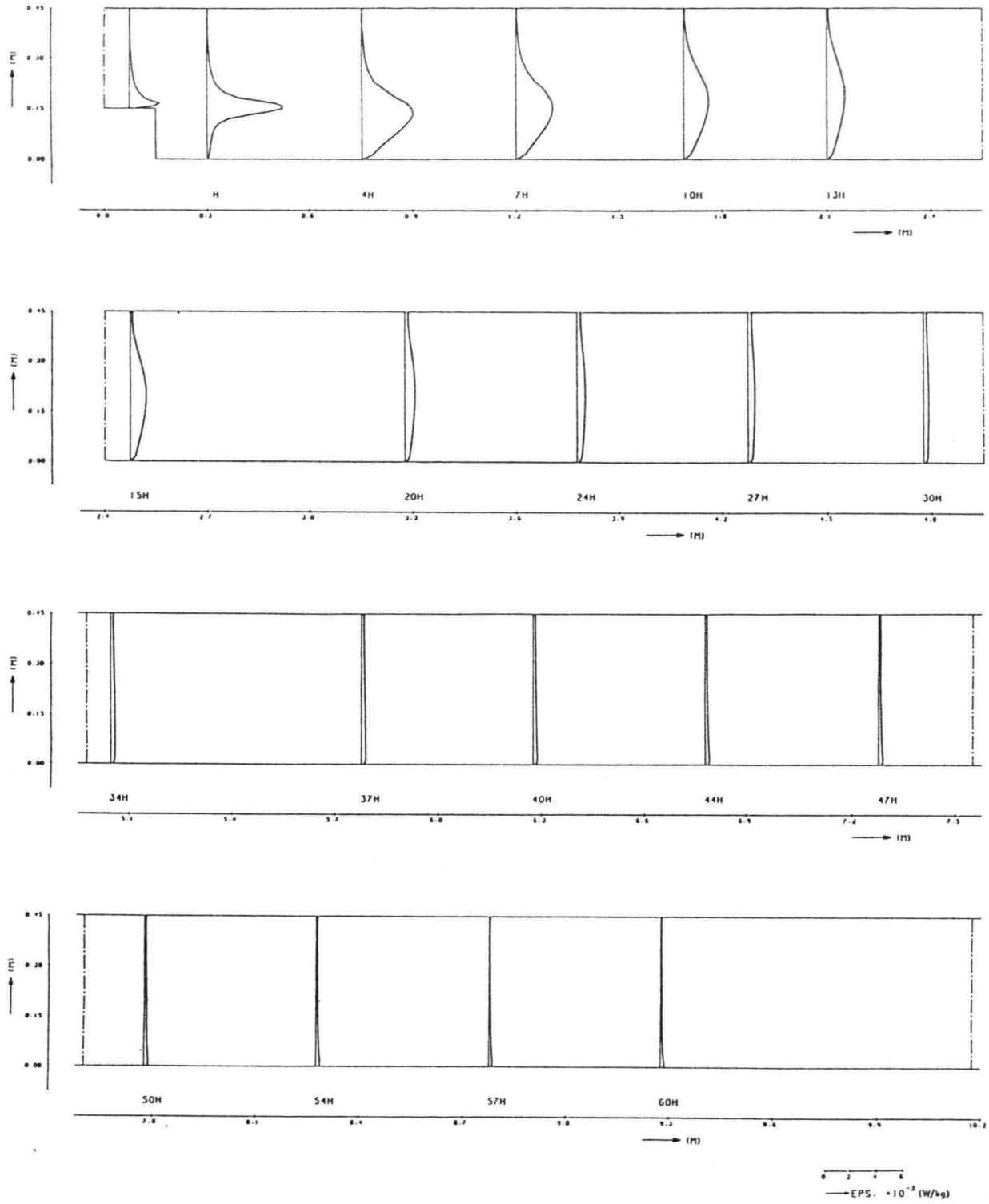

figure 9. Dissipation profiles ($k-\varepsilon$ predictions)

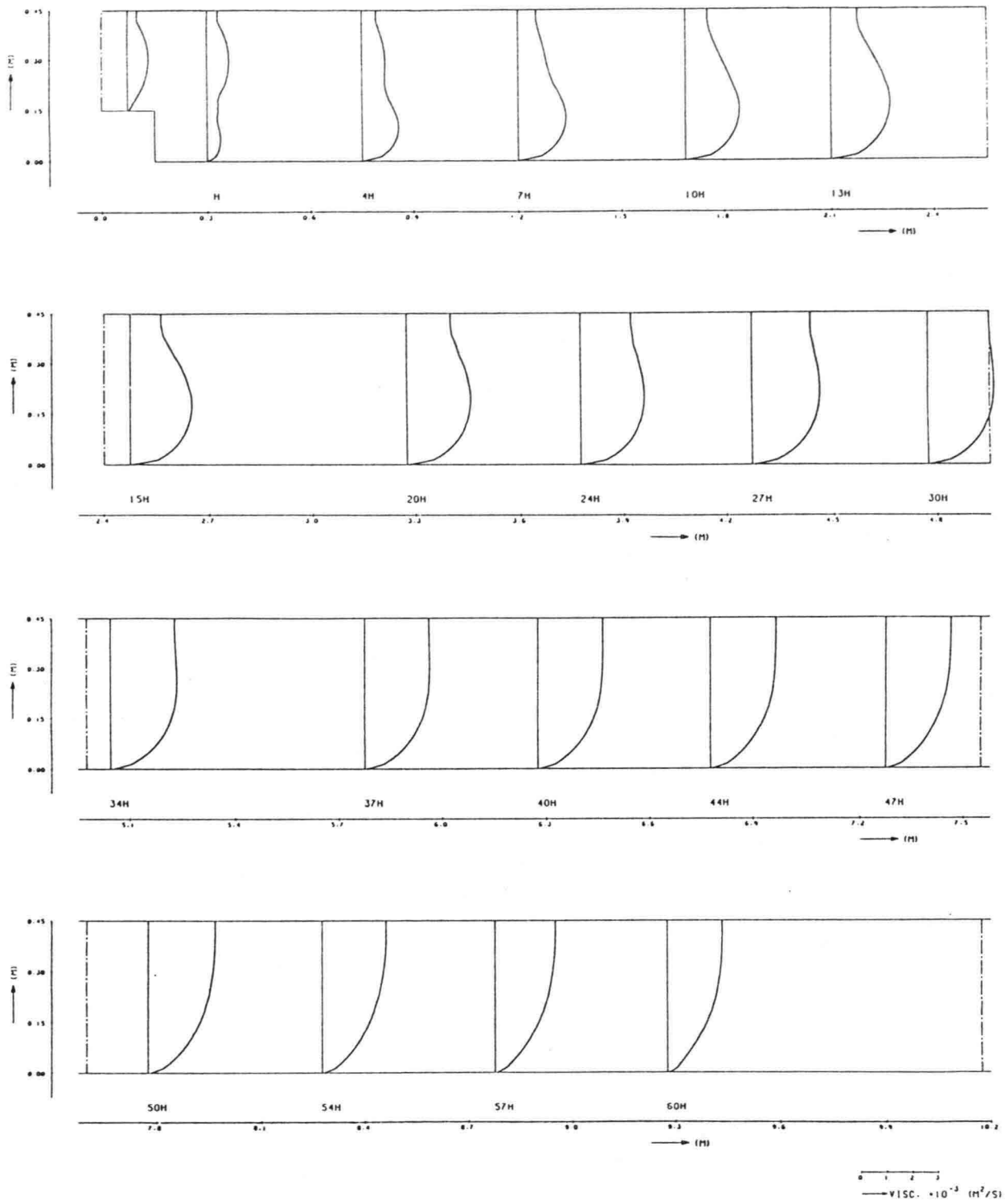

figure 10. Eddy viscosity profiles ($k-\varepsilon$ predictions)

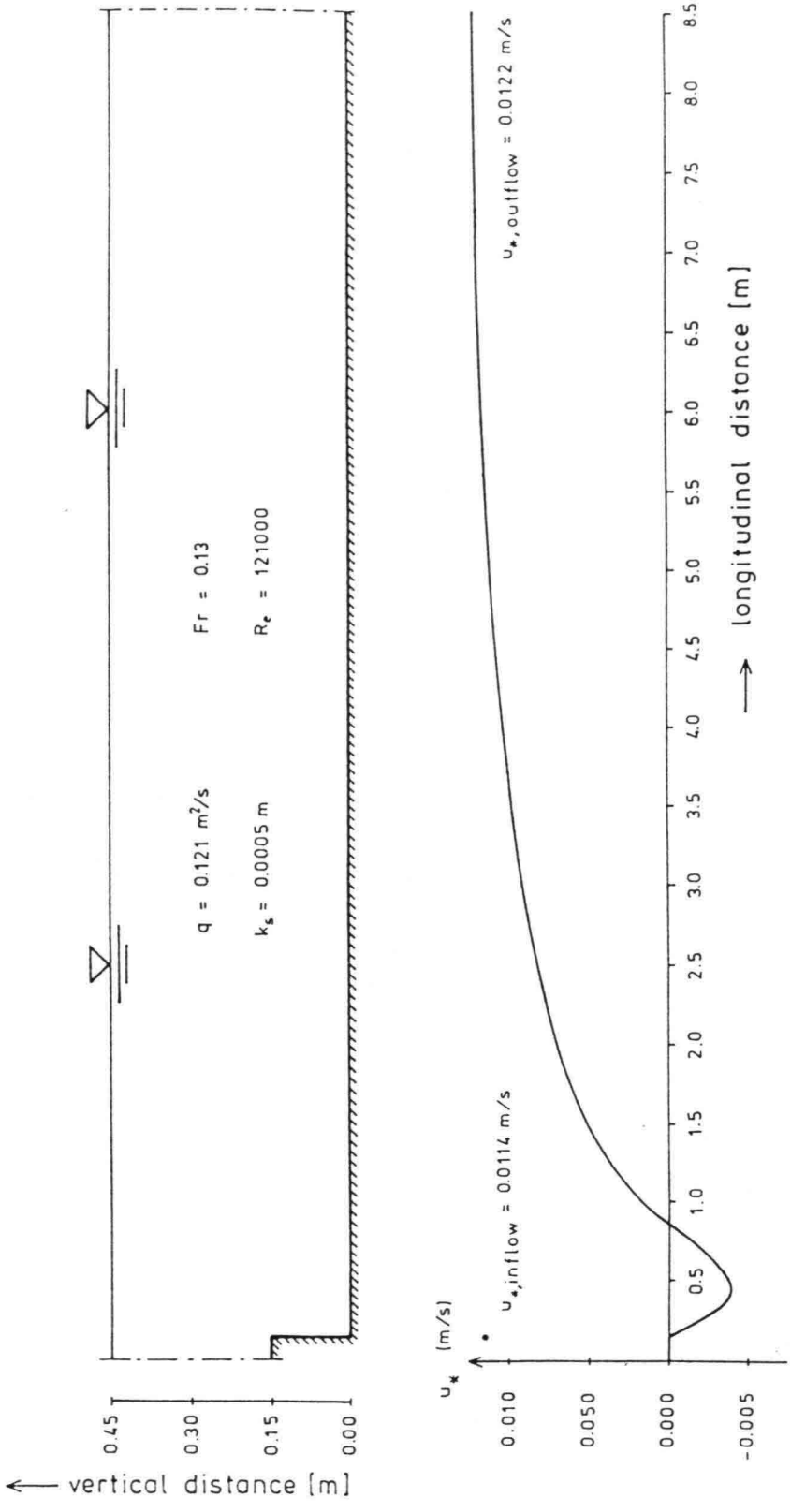

figure 11. Wall – shear – stress distribution (k – ε predictions)

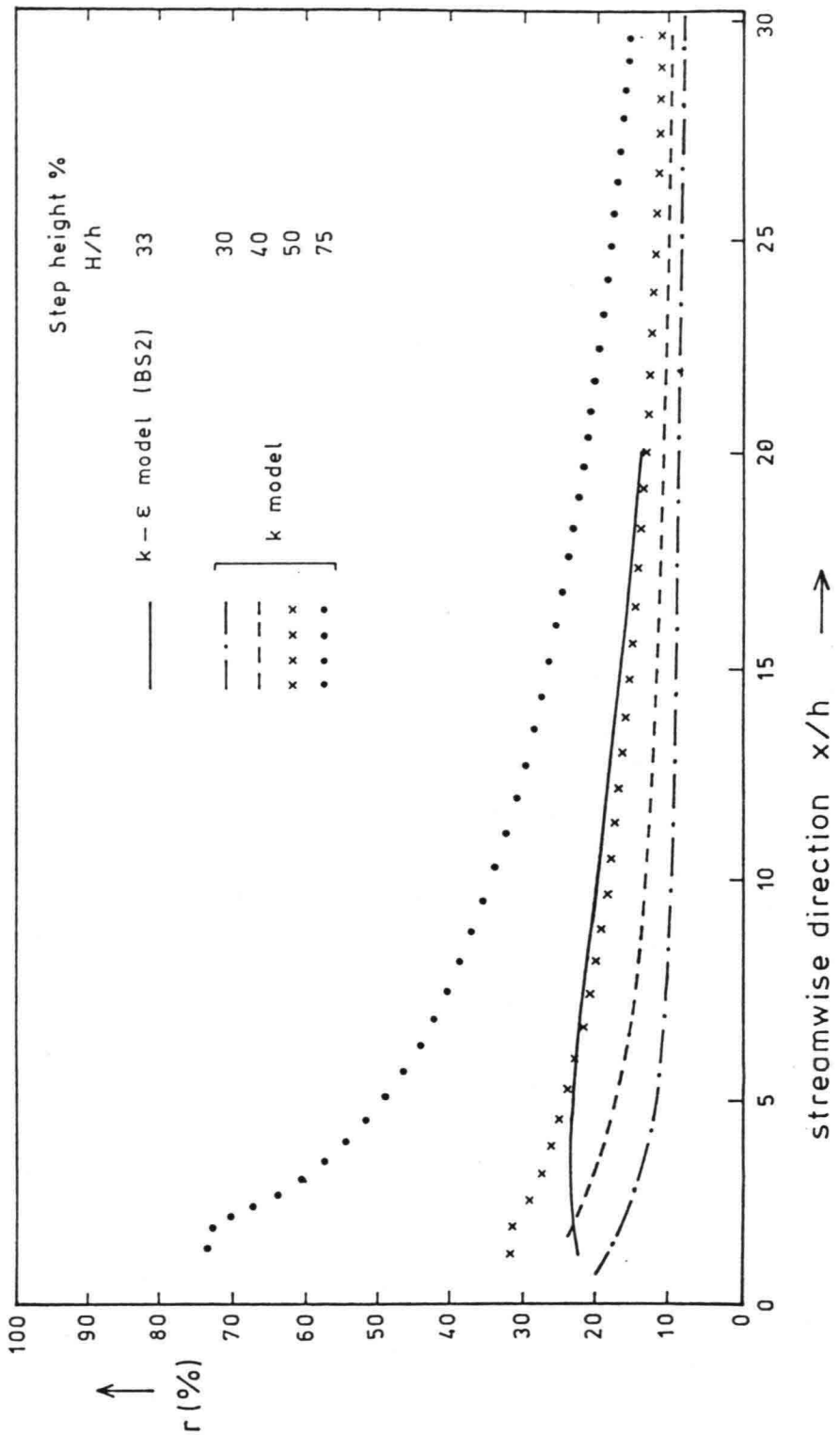

figure 12. Relative turbulence (r) against the streamwise direction (after a threshold).

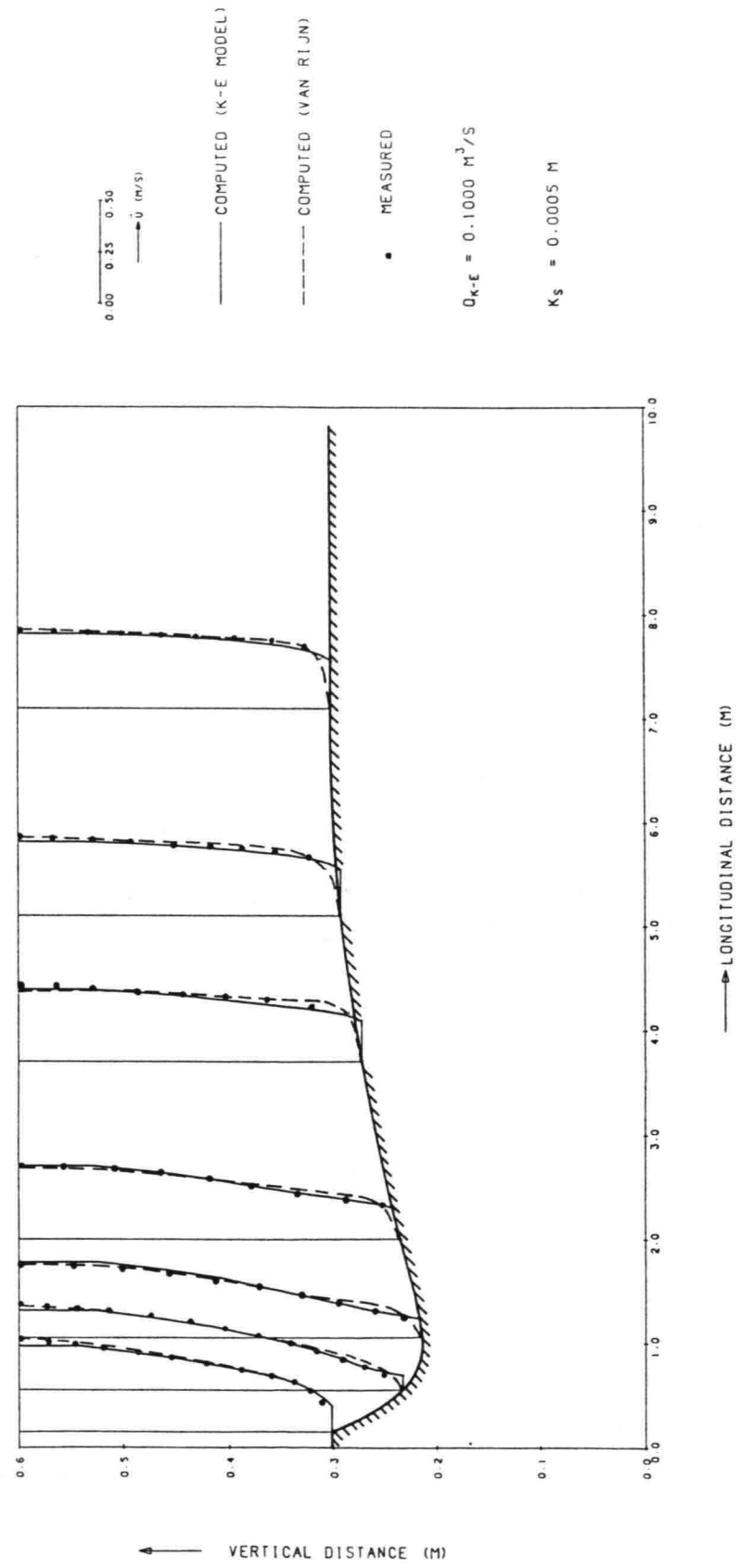

figure 13. Mean flow velocity profiles (LS 1)

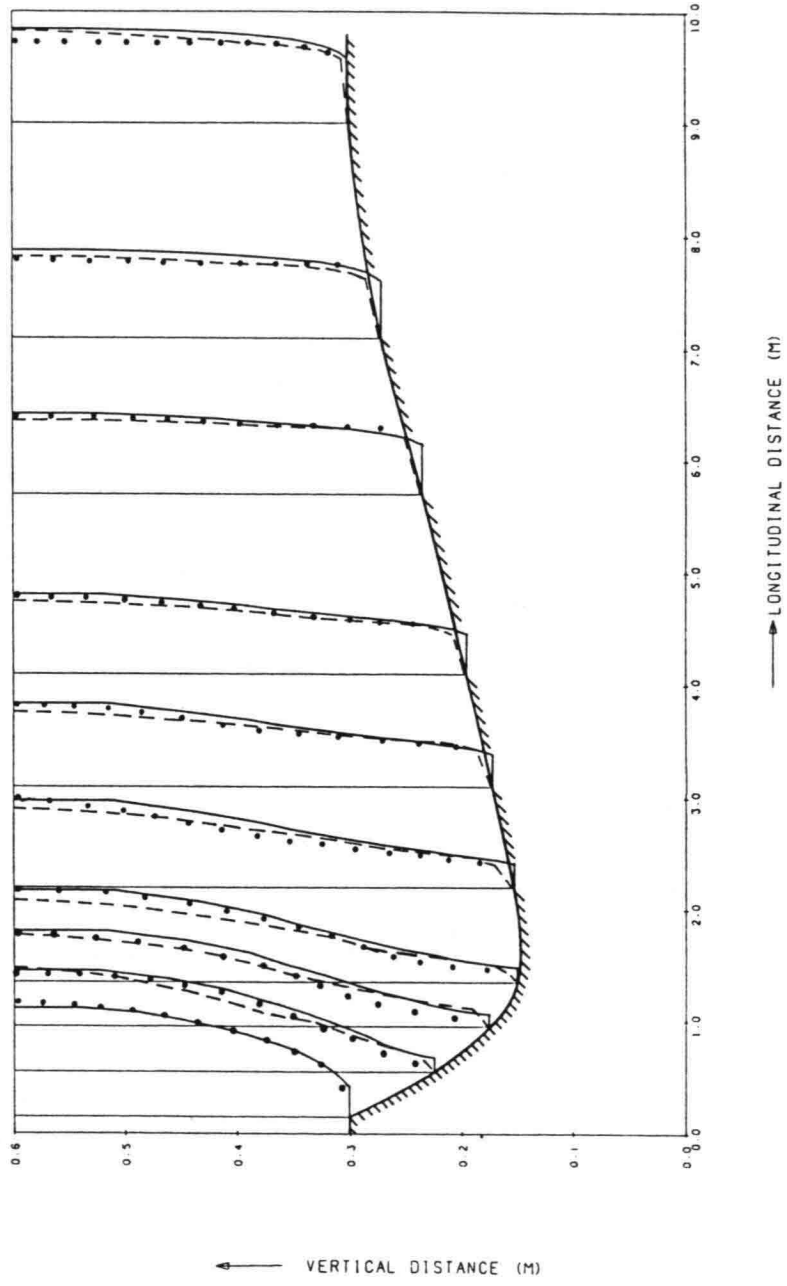

figure 14. Mean flow velocity profiles (LS 2)

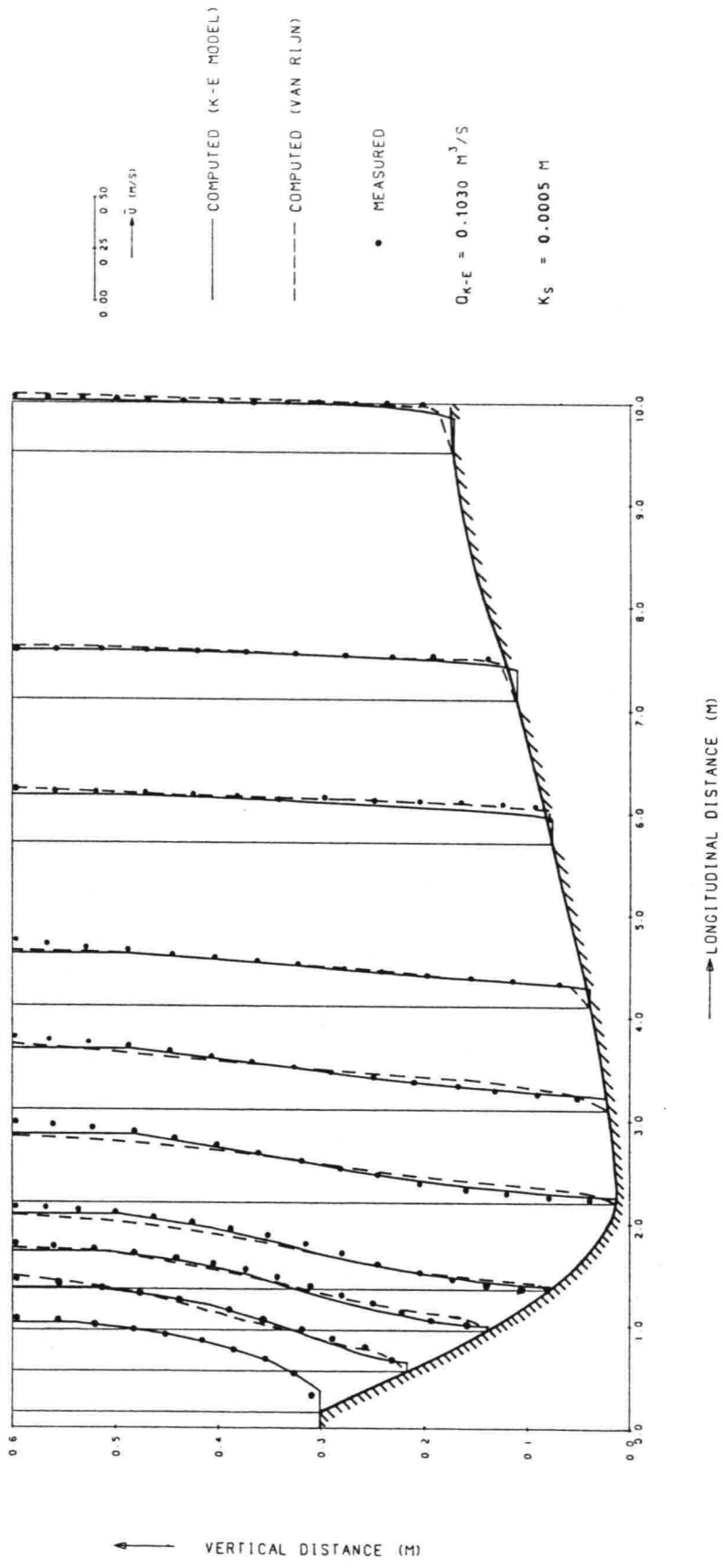

figure 15. Mean flow velocity profiles (LS 3)

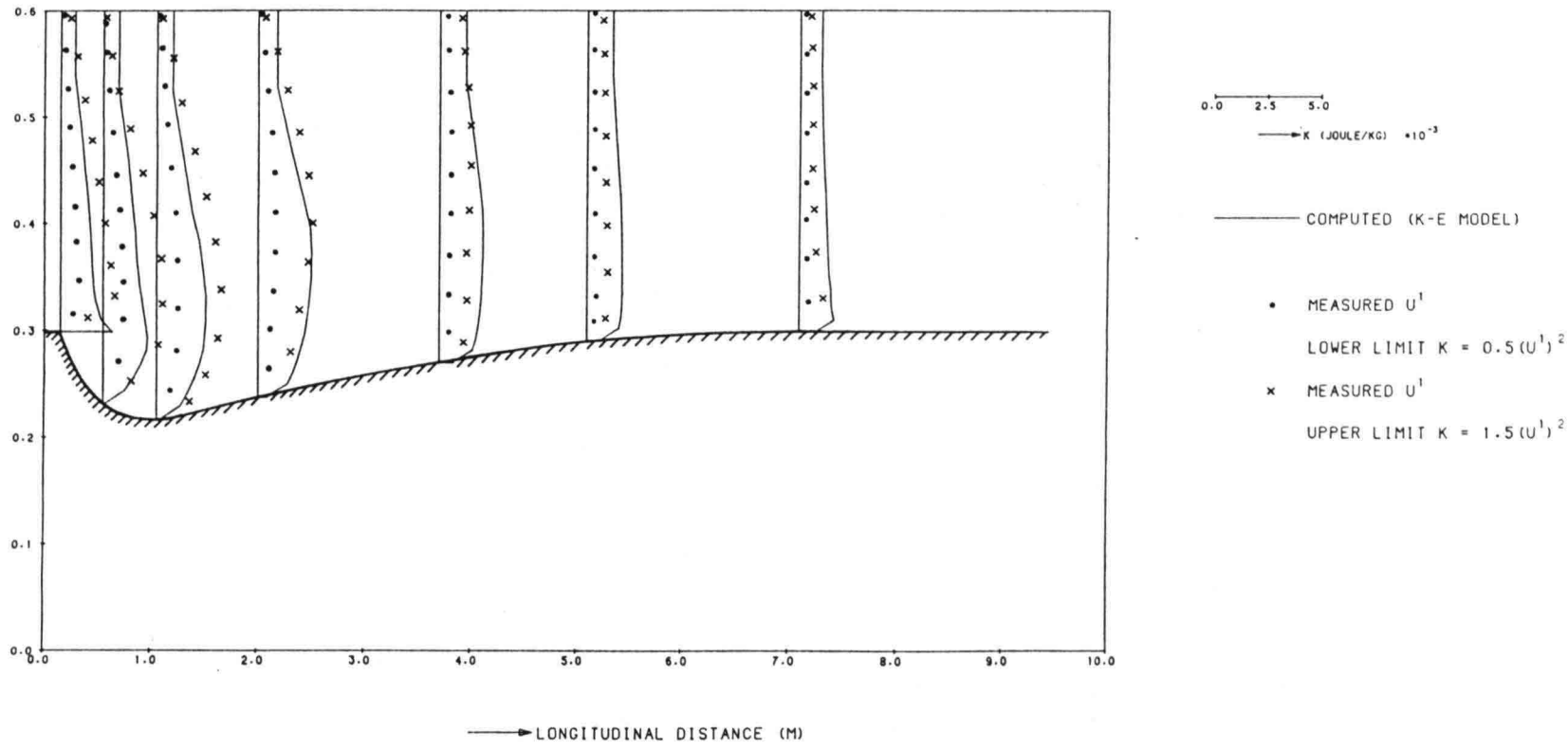

figure 16. Turbulence energy profiles (LS 1)

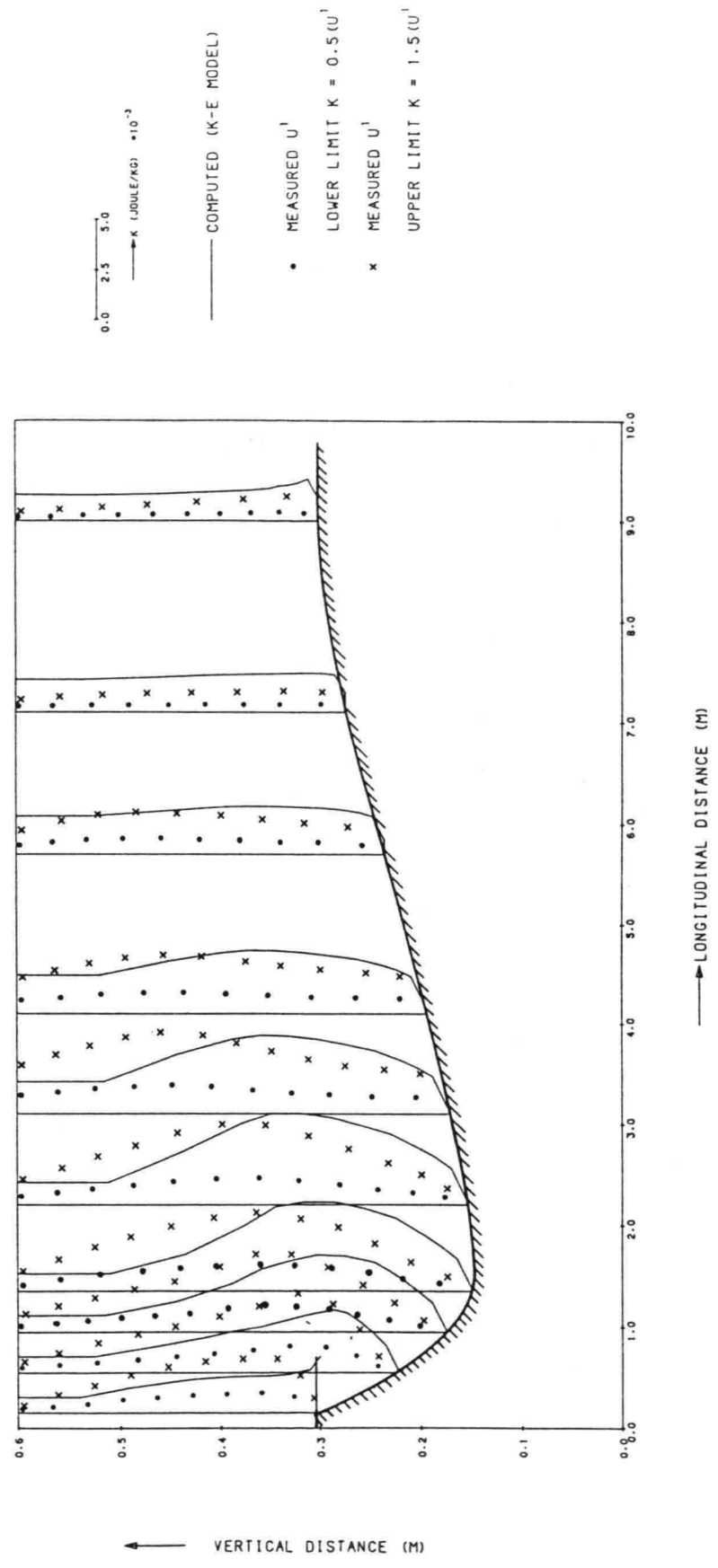

figure 17. Turbulence energy profiles (LS 2)

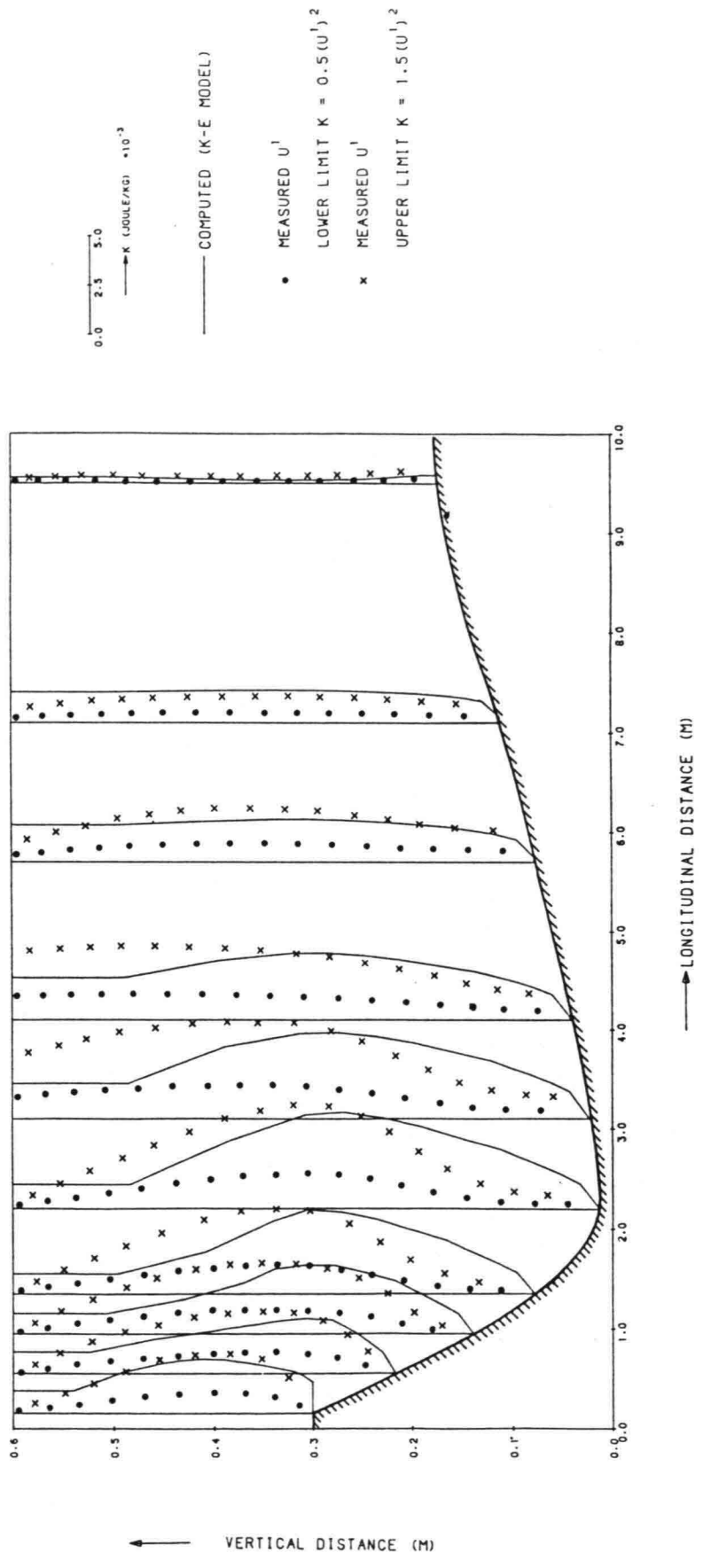

figure 18 Turbulence energy profiles (LS 3)

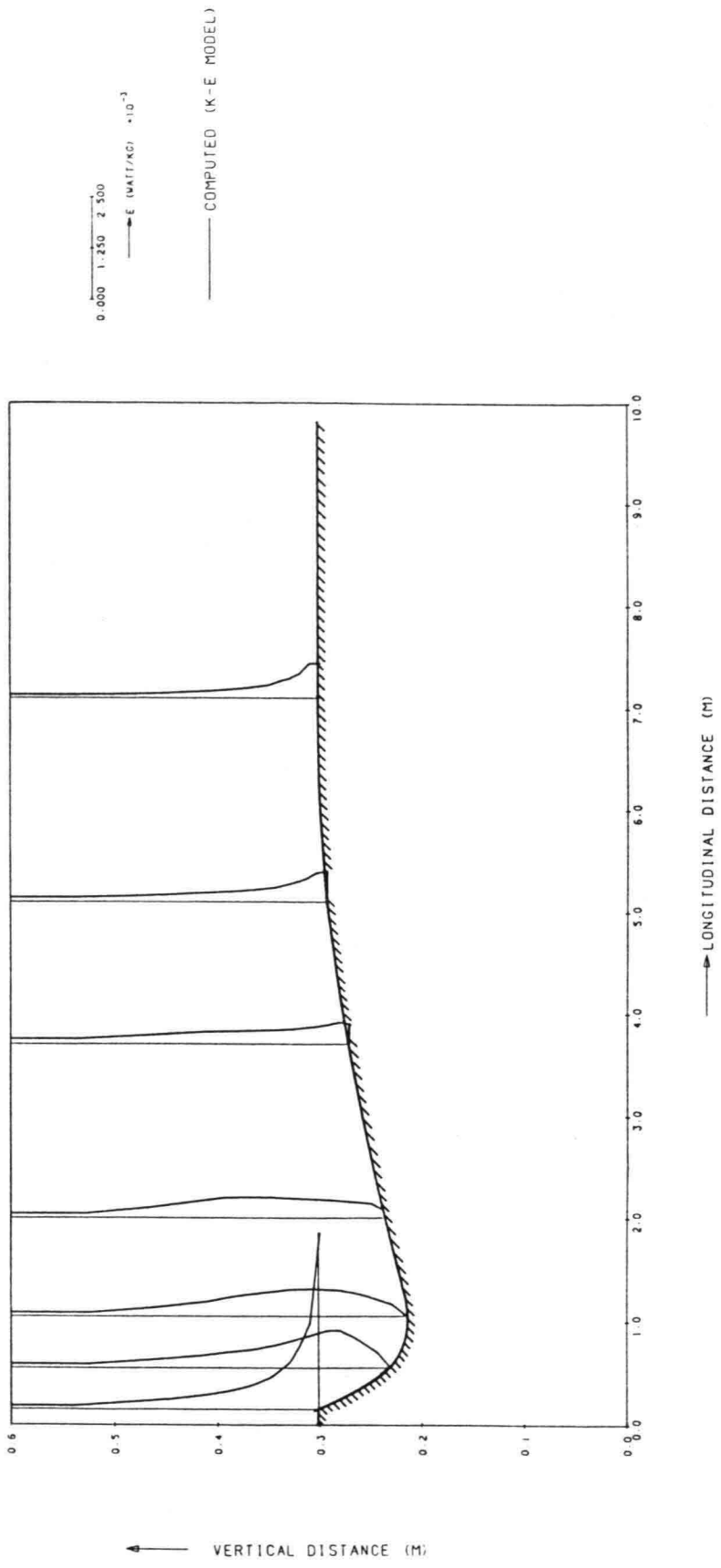

figure 19. Dissipation profiles (LS 1)

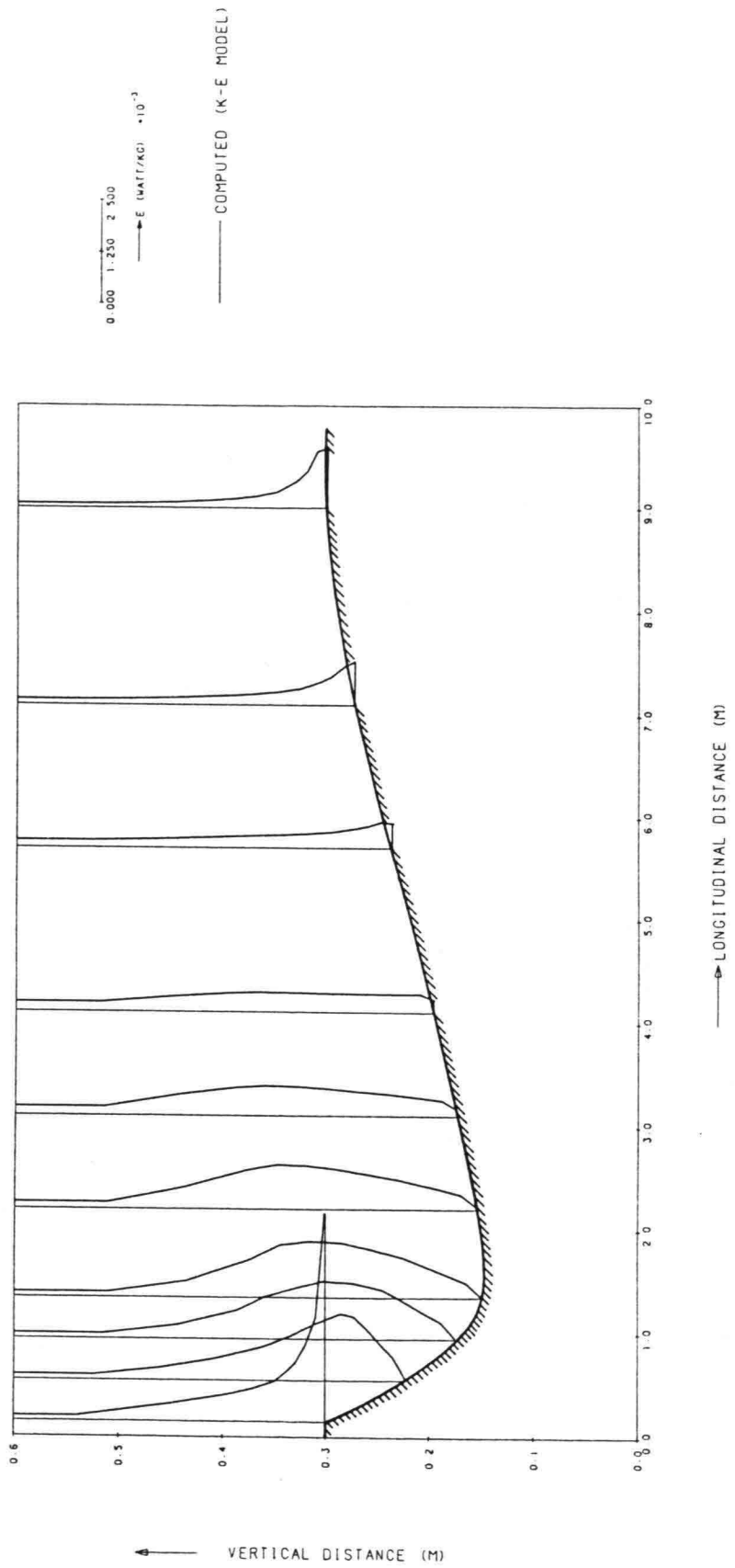

figure 20. Dissipation profiles (LS 2)

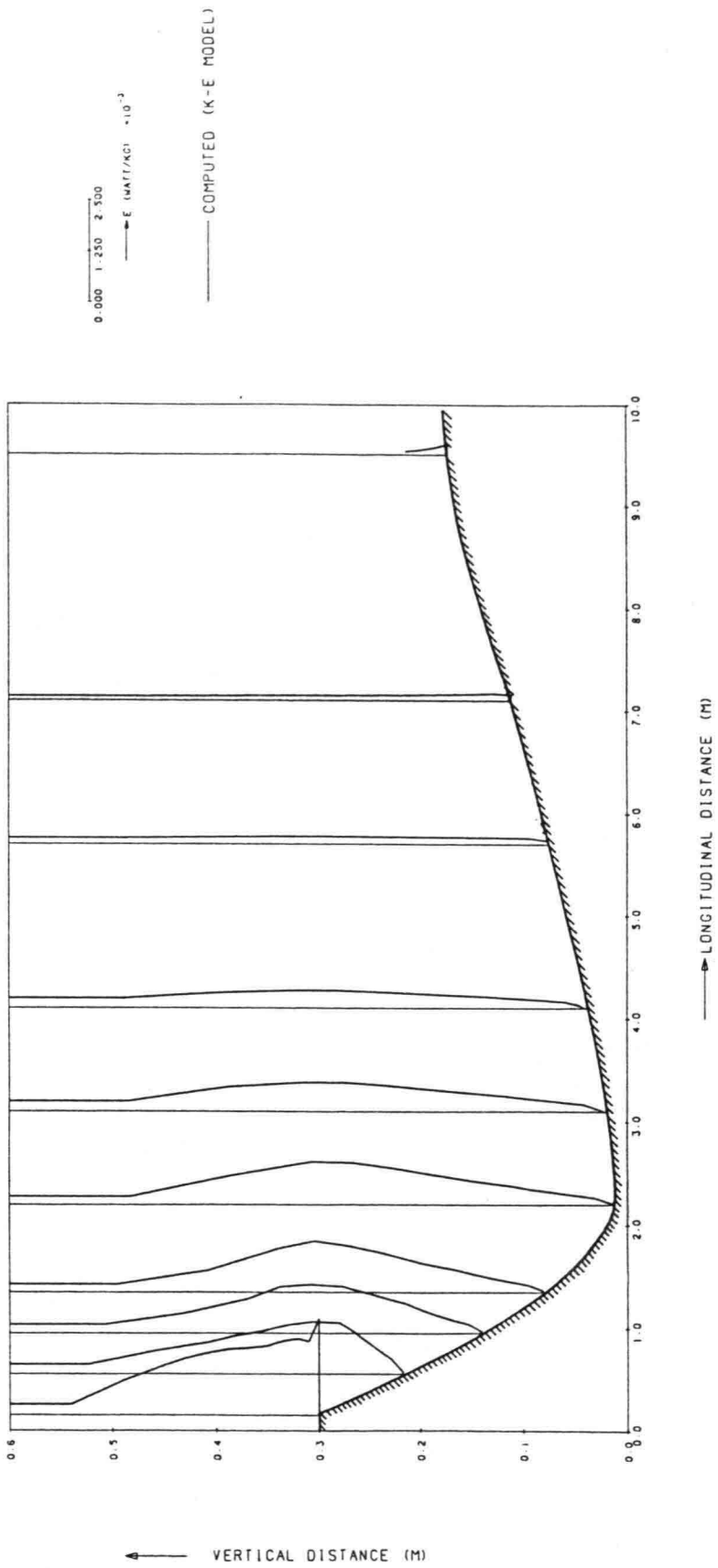

figure 21. Dissipation profiles (LS 3)

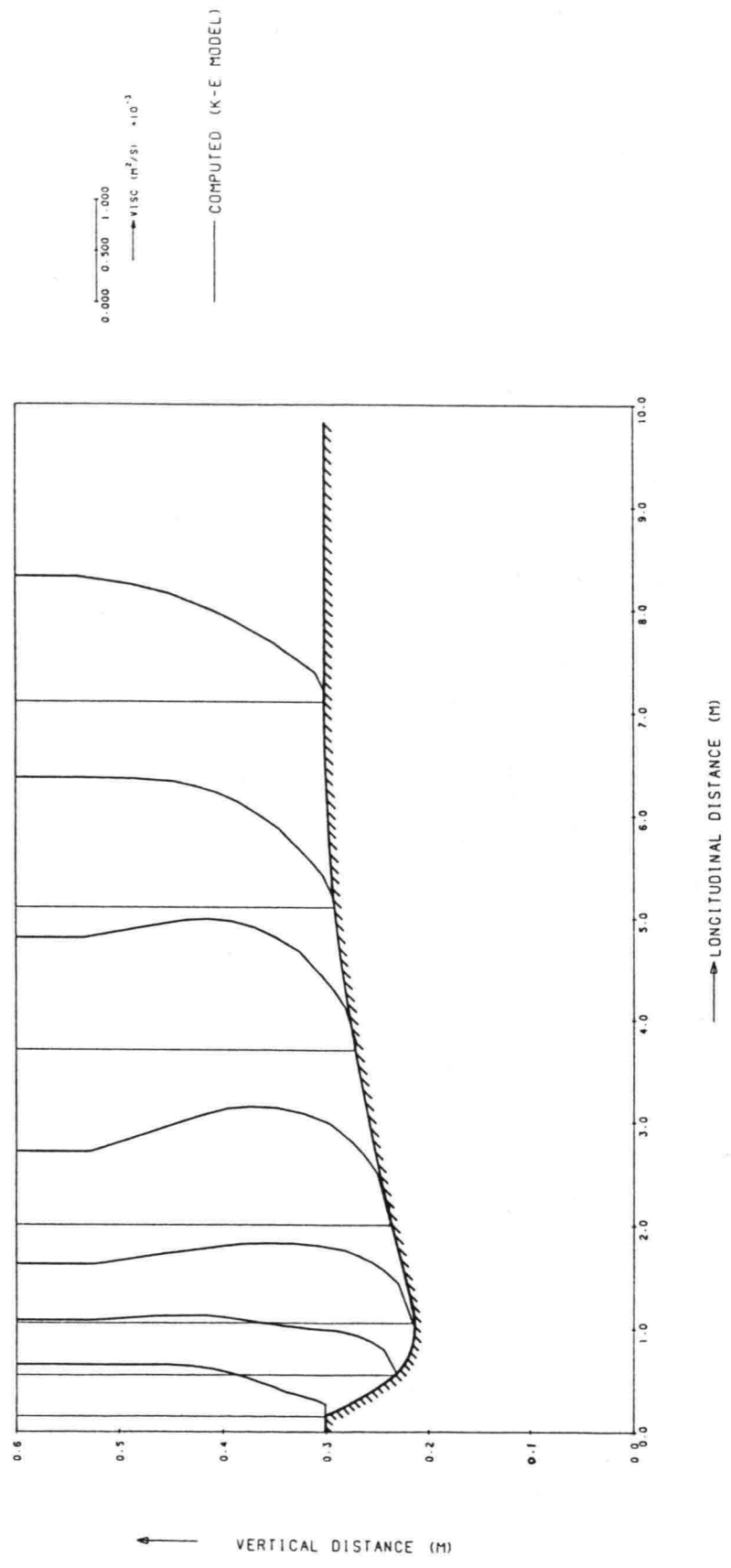

figure 22. Eddy viscosity profiles (LS 1)

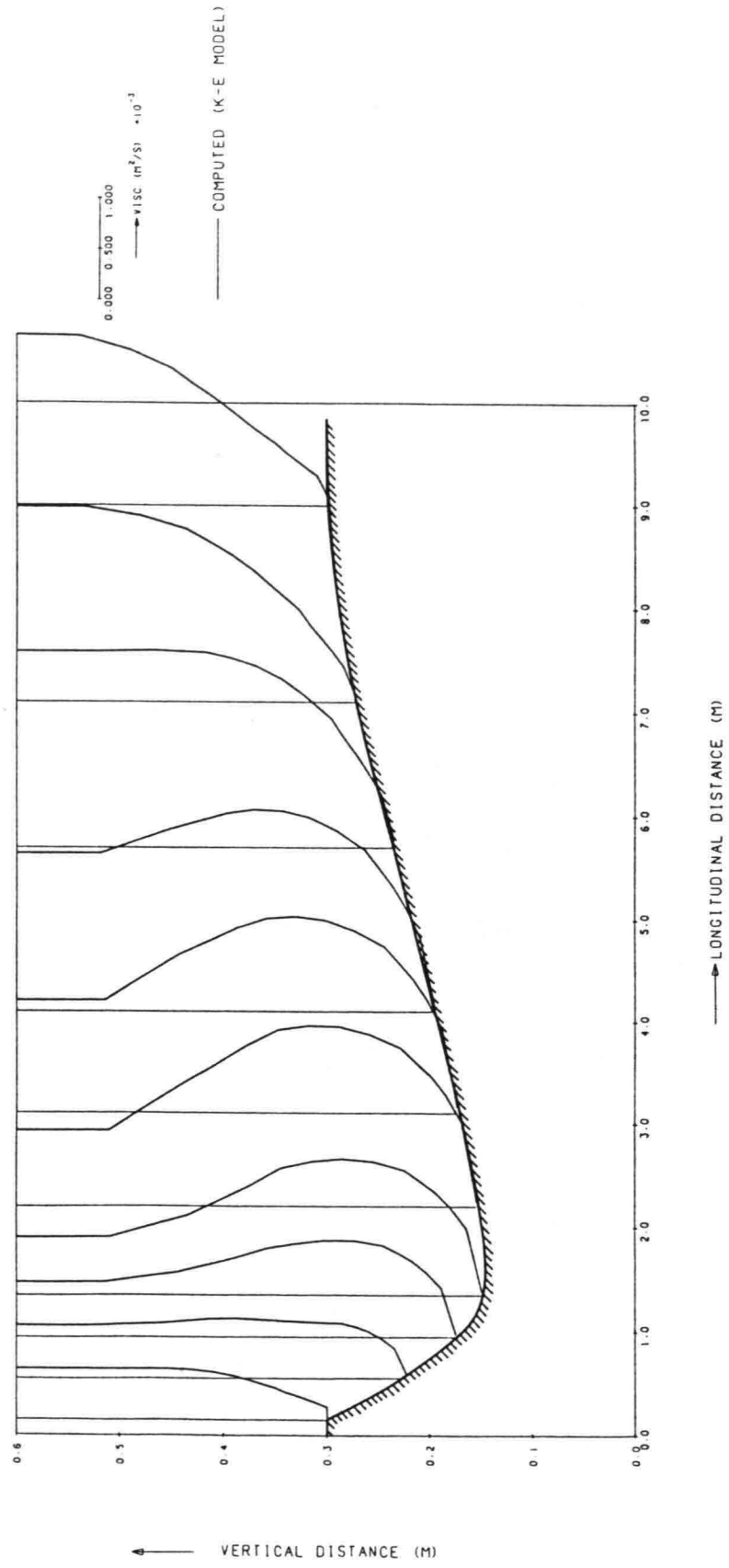

figure 23. Eddy viscosity profiles (LS 2)

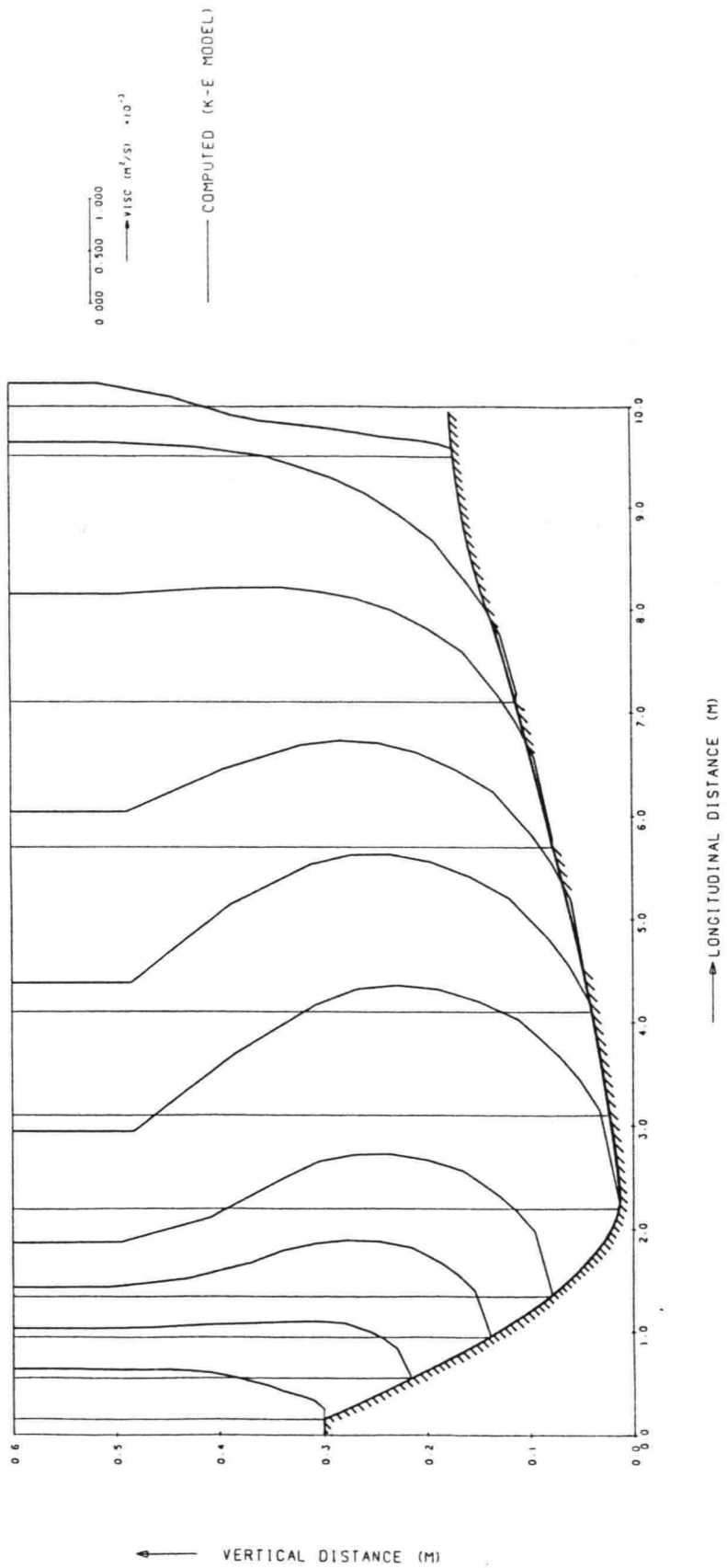

figure 24. Eddy viscosity profiles (LS 3)